

# Augmented Lagrangian Method based adjoint space framework for sparse reconstruction of acoustic source with boundary measurements

Nirui Tan\*      Hongpeng Sun†‡

October 17, 2025

## Abstract

We propose a semismooth Newton-based augmented Lagrangian method for reconstructing sparse sources in inverse acoustic scattering problems. The semismooth Newton method can be iterated in the space of measurements instead of the unknown source to be reconstructed. It is highly efficient, especially when the measurement data is much less than the acoustic source. The source can be calculated from Fenchel-Rockafellar duality theory. We can obtain lots of acceleration and leverage the computational cost. The numerical examples show the high efficiency of the proposed semismooth Newton-based methods.

## 1 Introduction

Inverse acoustic scattering is crucial in various applications, including sonar imaging, oil prospecting, and non-destructive testing, among others [17]. In this paper, we focus on the reconstruction of acoustic sources, which is a typical inverse acoustic scattering problem. It is well-known that the inverse source problem lacks uniqueness [8, 30] due to the presence of non-radiating sources, resulting in high ill-posedness. Appropriate regularization that incorporates prior information can leverage the ill-posedness, such as  $L^2$  regularization [19]. For convenience, we assume that  $\Omega \subseteq \mathbb{R}^d$  with  $d = 2$  or  $d = 3$  is a bounded and compact domain with boundary  $\partial\Omega$  of class  $C^3$  and contains the sources. Sparse regularization is a popular choice for signal processing, including  $L^1$  regularization and total variation, which can promote sparsity for the solutions or gradients. However, for acoustic scattering involving the Helmholtz equation, which is an infinite-dimensional problem, the existence

---

\*School of Mathematics, Renmin University of China, 100872 Beijing, China. Email: niruitan@ruc.edu.cn.

†School of Mathematics, Renmin University of China, 100872 Beijing, China. Email: hpsun@amss.ac.cn.

‡Corresponding author.

of a reconstructed solution in  $L^1(\Omega)$  space can not be guaranteed, due to the lack of weak completeness in  $L^1(\Omega)$  (see Chapter 4 of [10]). In [9, 15, 16], a larger space, the Radon measure space  $\mathcal{M}(\Omega)$ , is introduced for inverse problems and sparse optimal control. We also refer to [2] for inverse problems, including electrical impedance tomography with finite measurements and the linearized and locally optimized strategy and algorithms for sparse point acoustic sources [1].

It is known that  $\mathcal{M}(\Omega)$  is a Banach space and can be characterized by its dual space  $C_0(\Omega)$  through the Riesz representation theorem (see Chapter 4 of [10]),

$$\|\mu\|_{\mathcal{M}(\Omega)} = \sup \left\{ \int_{\Omega} u d\mu : u \in C_0(\Omega), \|u\|_{C_0(\Omega)} \leq 1 \right\}. \quad (1.1)$$

This is also equivalent to  $\mathcal{M}(\Omega) = C_0(\Omega)'$ , which means that  $\mathcal{M}(\Omega)$  is weakly compact by the Banach-Alaoglu theorem since  $C_0(\Omega)$  is a separable Banach space [10]. The existence of the reconstructed sparse solution in the Radon measure space  $\mathcal{M}(\Omega)$  can be guaranteed. Moreover, since  $L^1(\Omega)$  can be embedded in  $\mathcal{M}(\Omega)$ , the regularization with  $\mathcal{M}(\Omega)$  can also promote sparsity. Inspired by the developments of the Radon measure space regularization [15, 16], [32] considered the sparse reconstruction of an acoustic source in the Radon measure space  $\mathcal{M}(\Omega)$ . Full scattering data in  $\Omega$  is employed, and semismooth Newton is developed for reconstruction algorithms [32].

There are several iterative methods for inverse scattering with smooth functionals such as  $L^2$  regularization, including the gradient descent method [47], recursive linearization [5, 6], Newton-type methods, or distorted Born iteration [11, 24, 26, 27, 29, 39]. For non-smooth regularization, the primal-dual method for the total variation regularized inverse medium scattering problem is developed in [12, 13, 14]. Let us turn to a discrete setting for discussing the efficiency. Suppose that  $M$  is the number of unknowns modeling the scatter and  $N$  is the number of measurements. It is claimed that “For most practical situations, the number of unknowns is much larger than the number of measurements, i.e.,  $N \gg M$ ” in [11]. It was further pointed out that  $M \propto \sqrt{N}$  generally for the two-dimensional case [29]. Currently, these Newton-type or distorted Born-type methods are iterated directly in the domain of the unknowns, which means that a linear system such as  $Ax = b$  with  $A \in \mathbb{C}^{N \times N}$  has to be solved during each Newton update. It can be much more efficient if each Newton update can be carried out in the measurement domain by solving a linear system such as  $A_b z = c$  with  $A_b \in \mathbb{C}^{M \times M}$ . One then recovers the  $N$  unknowns through the  $M$  computed dual variables by the optimality conditions directly. This technique can reduce a lot of computational cost.

In this paper, we build a framework that the Newton or semismooth Newton executes on the measurement domain. We call the corresponding solution with the same dimensions of the measurements a “dual solution” or “adjoint field” [21]. We then recover the unknown acoustic source through Fenchel–Rockafellar duality theory. Our contributions can be summarized as follows. First, we develop a semismooth Newton-based augmented Lagrangian method, where we can employ semismooth Newton methods in the adjoint

space and the linear update of the Newton method to solve problems with the same dimensions as the boundary measurements. Such ideas for inverse electromagnetic scattering can be found in [21, 22], where incremental iterative methods are developed that involve a linear equation with the same dimensions as the measurements. Compared to [21, 22], our framework can handle nonsmooth regularization, whereas  $L^2$  Tikhonov regularization is employed in [21, 22]. The semismooth Newton method thus can be highly efficient, while the boundary measurements can be much less than the unknown acoustic source to be reconstructed. We would like to point out that a similar dual framework is studied for statistical or signal data processing [37, 48]. Second, we also design a semismooth Newton method with the Moreau–Yosida regularization [16, section 3.1], [28, Chapter 9] or [32] for directly reconstructing the acoustic source in case the scale of the measurement data is comparable with the unknowns.

The paper is organized as follows. In section 2, we introduce the direct problem. In section 3, we present the semismooth Newton-based augmented Lagrangian method in the adjoint space. In section 4, we introduce a semismooth Newton method and a first-order primal-dual method. In section 5, we present detailed numerical experiments both in two-dimensional and three-dimensional spaces. Finally, in section 6, we give a conclusion.

## 2 Inverse source problem with boundary measurements

In this paper, we will focus on the analysis and reconstruction of the following inverse scattering problem:

*Reconstructing a sparse source  $f$  in the Radon measure space  $\mathcal{M}(\Omega)$  for a given scattered field on the boundary  $\partial\Omega$ .*

The direct scattering problem in the frequency domain with an inhomogeneous medium in  $\mathbb{R}^d$  with  $d = 2$  or  $d = 3$  is as follows

$$\begin{cases} -\Delta u - k^2 n(x)u = \mu, & x \in \mathbb{R}^d, \\ \lim_{|x| \rightarrow \infty} |x|^{\frac{d-1}{2}} \left( \frac{\partial u}{\partial |x|} - iku \right) = 0, \end{cases} \quad (2.1)$$

where  $\mu \in \mathcal{M}(\Omega)$  is a Radon measure and  $n(x)$  is the refraction index. We refer to Figure 1 for an illustration. Henceforth, we assume  $n(x)$  is real, smooth, and compactly supported, i.e.,  $\Im n = 0$  and there exists a bounded domain  $\Omega \subseteq \mathbb{R}^d$  such that  $\text{supp}(n(x) - 1) \Subset \Omega$ . Throughout this paper, we assume  $\mu$  is a real Radon measure, which is reasonable in physics and is also compactly supported. We assume the bounded domain  $\Omega$  is large enough such that  $\mu$  is also compactly supported in  $\Omega$ , i.e.,  $\text{supp}(\mu) \Subset \Omega$ . The Helmholtz equation (2.1) can also be recovered with  $n(x) \equiv 1$ .

The solution of (2.1) is defined in “very weak” sense [32, Definition 2.1] with test functions in  $C^{2,\alpha}$ . Here, for convenience, we directly work with the following volume

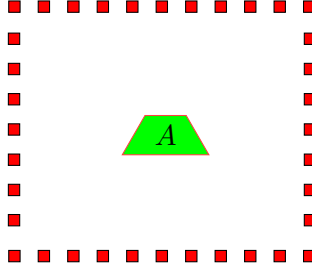


**Figure 1:** Illustration of the acoustic source scattering: the red squares represent the receivers for recording the scattering wave, and the trapezoid  $A$  represents the acoustic sources.

potential representations,

$$(\mathcal{V}\mu)(x) := \int_{\Omega} G(x, y) d\mu(y), \quad (2.2)$$

where the inhomogeneous and background Green's function  $G(x, y)$  is defined as the radiating solution [18]

$$\begin{cases} -\Delta_x G(x, y) - k^2 n(x) G(x, y) = \delta(x - y), & x, y \in \mathbb{R}^d, \\ \lim_{|x| \rightarrow \infty} |x|^{\frac{d-1}{2}} \left( \frac{\partial G(x, y)}{\partial |x|} - ikG(x, y) \right) = 0. \end{cases} \quad (2.3)$$

Denoting  $m(x) = 1 - n(x)$ , we thus can construct  $G(x, y)$  by the Lippmann-Schwinger integral equation [18]

$$G(x, y) = \Phi(x, y) - k^2 \int_{\Omega} \Phi(x, z) m(z) G(z, y) dz \quad (2.4)$$

where  $\Phi(x, y)$  is the fundamental solution of the Helmholtz equation, i.e.,  $\Phi(x, y) = \frac{i}{4} H_0^{(1)}(k|x - y|)$  in  $\mathbb{R}^2$  and  $\Phi(x, y) = \frac{e^{ik|x-y|}}{4\pi|x-y|}$  in  $\mathbb{R}^3$ . For the  $W^{1,p}$  estimate of the problem (2.1), we have the following proposition [32, Theorem 2.8].

**Proposition 1.** *For the solution of (2.1) with representation in (2.2), we have the following regularity estimate,*

$$\|u\|_{W^{1,p}(\Omega)} \leq C\|\mu\|_{\mathcal{M}(\Omega)}, \quad 1 \leq p < \frac{d}{d-1}, \quad d = 2 \text{ or } d = 3. \quad (2.5)$$

Here  $C$  is a positive constant that does not depend on  $\mu$ .

According to the trace theorem of  $W^{1,p}(\Omega)$  in [4, Theorem 5.36], we have

$$W^{1,p}(\Omega) \hookrightarrow L^s(\partial\Omega), \quad p \leq s \leq s^* = (d-1)p/(d-p) = (d-1)/(\frac{d}{p} - 1). \quad (2.6)$$

Since  $p < d/(d-1)$  as in (2.5), we have the estimate on  $s$

$$s = \begin{cases} s_0, & \forall s_0, \text{ such that } p \leq s_0 < \infty, \quad d = 2, \\ s_0, & \forall s_0, \text{ such that } p \leq s_0 < 2, \quad d = 3. \end{cases} \quad (2.7)$$

With the above trace property (2.6), to reconstruct the sparse source  $\mu \in \mathcal{M}(\Omega)$ , we will make use of the following sparse regularization functional,

$$\min_{\mu} \frac{1}{2} \|\mathcal{V}\mu - u_b\|_{L^s(\partial\Omega)}^2 + \alpha \|\mu\|_{\mathcal{M}(\Omega)}, \quad \forall s \begin{cases} \text{such that } p \leq s < \infty, & d = 2, \\ \text{such that } p \leq s < 2, & d = 3, \end{cases} \quad (2.8)$$

where  $\alpha$  is the regularization parameter and  $u_b$  is the measured scattered fields on  $\partial\Omega$ .  $\mathcal{V}\mu$  satisfies the equation (2.1) as discussed.

**Theorem 1.** *There exists a solution  $\mu \in \mathcal{M}(\Omega)$  of the regularization functional (2.8).*

*Proof.* The proof is similar to [16, Proposition 2.2] and [9]. Since the energy in (2.8) is  $\frac{1}{2} \|u_b\|_{L^s(\partial\Omega)}^2$  while  $\mu = 0$ . Thus we can find a minimizing sequence  $\{\mu_n\}$  in  $\mathcal{M}(\Omega)$  which are bounded by  $\frac{1}{2\alpha} \|u_b\|_{L^s(\partial\Omega)}^2$ . Since  $\mathcal{M}(\Omega)$  is a weakly sequentially compact [10] (see Chapter 4), there exists a weakly convergent subsequence  $\mu_{n,k}$  converging to  $\mu^* \in \mathcal{M}(\Omega)$  weakly.

Denoting  $u_{n,k} = \mathcal{V}(\mu_{n,k})$ , we see  $u_{n,k} \in W^{1,p}(\Omega)$  with  $p < \frac{d}{d-1}$ . By Proposition 1,  $u_{n,k}$  weakly converges to  $\mathcal{V}(\mu^*)$  and  $\mathcal{V}(\mu^*)$  is a solution (2.1) within definition of the very weak solution [32, Definition 2.1] defined as the dual of  $C^{2,\alpha}$ . By the weak lower semicontinuity of the norms in  $L^2(\Omega)$  and  $\mathcal{M}(\Omega)$ , we conclude that  $\mu^*$  is a minimizer of (2.8) and the existence follows.  $\square$

For the non-smooth minimization problem (2.8), it is convenient to consider the predual problem under the powerful Fenchel–Rockafellar duality theory; see [9, 15, 16, 28] for its various applications in inverse problems and optimal control problems. The semismooth Newton method can be employed to compute dual problems efficiently. However, the problem (2.8) is with a complex-valued function. For the application of Fenchel–Rockafellar duality theory, we need to reformulate the complex-valued operators and functions in terms of real matrix operators and real vector functions. Let us denote

$$\mathcal{V} = \mathcal{V}_R + i\mathcal{V}_I \text{ with } V = \begin{pmatrix} \mathcal{V}_R & -\mathcal{V}_I \\ \mathcal{V}_I & \mathcal{V}_R \end{pmatrix}, \quad \mu := \begin{pmatrix} \mu_R \\ \mu_I \end{pmatrix}, \text{ and } u_b := \begin{pmatrix} \Re u_b \\ \Im u_b \end{pmatrix}, \quad (2.9)$$

where  $\mathcal{V}_R = \Re(\mathcal{V})$ ,  $\mathcal{V}_I = \Im(\mathcal{V})$ . We still employ  $\mu$  and  $u_b$  as their complex realization.

### 3 Semismooth Newton-based Augmented Lagrangian Method

Henceforth, we consider the discrete setting of the functional in (2.8) and denote  $\mathcal{V}_b = V|_{\partial\Omega}$ , i.e, the trace of the volume potential after complex realization. For the discretization of  $\mathcal{V}_b$ ,

we employ the framework in [31], which is implemented in [12, 13] with publicly available code. The inhomogeneous medium can be solved by the Lippmann-Schwinger equation; we will leave some comments in section 5. Since  $\mathcal{V}_b$  may lack of injectivity, for the convenience of the semismooth Newton methods along with optimization framework, we introduce an extra  $L^2$  regularization, and work in  $L^2(\partial\Omega)$  instead of  $L^s(\partial\Omega)$  in discrete settings,

$$\min_{\mu} \mathcal{P}(\mu), \quad \mathcal{P}(\mu) := \frac{1}{2} \|\mathcal{V}_b\mu - u_b\|_{L^2(\partial\Omega)}^2 + \frac{\alpha_0}{2} \|\mu\|_{L^2(\Omega)}^2 + \alpha \|\mu\|_{L^1(\Omega)}. \quad (3.1)$$

In (3.1), we also replace  $\mathcal{M}(\Omega)$  by  $L^1(\Omega)$  since these two norms are equal in a discrete setting. Now, let us turn to the augmented Lagrangian method for solving (3.1). First, set

$$h(y) = \frac{1}{2} \|y - u_b\|_{L^2(\partial\Omega)}^2, \quad p(\mu) = \frac{\alpha_0}{2} \|\mu\|_{L^2(\Omega)}^2 + \alpha \|\mu\|_{L^1(\Omega)}. \quad (3.2)$$

Let us first present the general Fenchel-Rockafellar duality theory [28, Theorem 4.34] or [7, Theorem 15.23]. Let  $f, g$  be convex, proper, lower-semicontinuous functions in Hilbert spaces  $Y$  and  $X$ , and  $\Lambda : X \rightarrow Y$  is a linear, bounded, and continuous operator. Then, under certain conditions (such as  $0 \in \text{sri}(\text{dom } f - \Lambda(\text{dom } g))$  [7, Theorem 15.23] with “sri” denoting strong relative interior and  $\text{dom}$  denoting the definition domain), the dual problem of the following primal minimization problem

$$\min_x f(\Lambda x) + g(x) \quad (3.3)$$

is

$$\sup_y (-f^*(y) - g^*(-\Lambda^* y)) \Leftrightarrow \inf_y f^*(y) + g^*(-\Lambda^* y) \quad (3.4)$$

and we have the following properties on the optimal solutions  $(x^*, y^*)$

$$\begin{aligned} f(\Lambda x^*) + g(x^*) &= -f^*(y^*) - g^*(-\Lambda^* y^*), \\ \Lambda x^* &\in \partial f^*(y^*), \quad -\Lambda^* y^* \in \partial g(x^*). \end{aligned} \quad (3.5)$$

Here  $x^*$  and  $y^*$  are the solutions of the primal problem (3.3) and dual problem (3.4) respectively.  $\Lambda^* : X \rightarrow Y$  is the adjoint operator of  $\Lambda$ . The optimality conditions (3.5) can shuttle solutions between the primal and the dual solutions.

We will first present the semismooth Newton-based augmented Lagrangian method, followed by the convergence analysis.

### 3.1 Semismooth Newton-based augmented Lagrangian framework in the dual space

Now let us turn to (3.1). It can be reformulated as

$$\min_{\mu} h(\mathcal{V}_b\mu) + p(\mu). \quad (3.6)$$

By direct calculations, we see that the dual functions of  $h$  and  $p$  are

$$h^*(y) = \frac{1}{2} \|y\|_{L^2(\partial\Omega)}^2 + \langle y, u_b \rangle_{L^2(\partial\Omega)}, \quad (3.7)$$

and

$$p^*(z) = \langle z', z \rangle_{L^2(\Omega)} - \frac{\alpha_0}{2} \|z'\|_{L^2(\Omega)}^2 - \alpha \|z'\|_{L^1(\Omega)}, \quad z' = \mathcal{S}_{\frac{\alpha_1}{\alpha_0}}\left(\frac{z}{\alpha_0}\right), \quad (3.8)$$

where  $\mathcal{S}$  is the soft thresholding operator

$$[\mathcal{S}_\sigma(z)]_i := \begin{cases} 0, & |z_i| \leq \sigma \\ z_i - \sigma \text{sign}(z_i), & |z_i| > \sigma \end{cases} \quad (3.9)$$

and  $\text{sign}(\cdot)$  is the sign function. It will turn out that the explicit formulation of  $p^*$  is not needed later. By Fenchel–Rockafellar duality, we obtain the dual problem of (3.6)

$$\min_{y \in L^2(\partial\Omega)} \mathcal{D}(y) := p^*(-\mathcal{V}_b^T y) + h^*(y), \quad (3.10)$$

which is equivalent to  $\max_{y \in L^2(\partial\Omega)} (-p^*(-\mathcal{V}_b^T y) - h^*(y))$  by (3.4). Furthermore, letting  $-\mathcal{V}_b^T y = z$ , the above minimization problem becomes the following linear constrained optimization problem

$$\min_{y \in L^2(\partial\Omega), z \in L^2(\Omega)} p^*(z) + h^*(y), \quad \text{s.t.}, \quad \mathcal{V}_b^T y + z = 0. \quad (3.11)$$

We now introduce the augmented Lagrangian function

$$L_\sigma(y, z; \lambda) := p^*(z) + h^*(y) + \langle \lambda, \mathcal{V}_b^* y + z \rangle_{L^2(\Omega)} + \frac{\sigma}{2} \|\mathcal{V}_b^T y + z\|_{L^2(\Omega)}^2. \quad (3.12)$$

We arrive at the following equivalent inf-sup problem for (3.6) under certain conditions,

$$\inf_{y \in L^2(\partial\Omega), z \in L^2(\Omega)} \sup_{\lambda \in L^2(\Omega)} L_\sigma(y, z; \lambda). \quad (3.13)$$

The augmented Lagrangian method thus follows, with nondecreasing update of  $\sigma_k \rightarrow c_\infty < +\infty$ , e.g.,  $\sigma_{k+1} = c_0 \sigma_k$ , where  $c_0 \in [2, 10]$  is a constant,

$$(y^{k+1}, z^{k+1}) = \arg \min_{y \in L^2(\partial\Omega), z \in L^2(\Omega)} L_{\sigma^k}(y, z; \lambda^k), \quad (3.14a)$$

$$\lambda^{k+1} = \lambda^k + \sigma_k (\mathcal{V}_b^T y^{k+1} + z^{k+1}). \quad (3.14b)$$

The Augmented Lagrangian method (shortened ALM) differs from ADMM (alternating direction method of multipliers), as ALM solves  $(y, z)$  variables together, whereas ADMM solves  $y$  and  $z$  separately. ALM can be obtained from the proximal point algorithm [41] to

the dual problem [42], and increasing the step sizes  $\sigma_k$  can obtain superlinear convergence for certain functions. For the developments of ALM, we refer to [35, 38] and [33, 34].

Semismooth Newton methods [28, 49] are widely employed for the nonlinear and non-smooth updates of ALM [37, 50] and [25, 36, 44]. For its application in total variation (or total generalized variation) regularized imaging processing problems, we refer to [45, 46]. Let us turn to semismooth Newton methods for solving the coupled nonlinear system of  $(y, z)$  in (3.14). The first order optimality conditions on  $y^{k+1}$  and  $z^{k+1}$  respectively of (3.14) tell that

$$\nabla h^*(y^{k+1}) + \mathcal{V}_b \lambda^k + \sigma \mathcal{V}_b (\mathcal{V}_b^T y^{k+1} + z^{k+1}) = 0, \quad (3.15)$$

$$\partial p^*(z^{k+1}) + \lambda^k + \sigma_k (z^{k+1} + \mathcal{V}_b^T y^{k+1}) \ni 0. \quad (3.16)$$

Usually, for discretizations, the dimensions of  $L^2(\partial\Omega)$  is much less than the dimensions of  $L^2(\Omega)$  [11]. It can be much more efficient if only the Newton update of  $y^{k+1}$  is solved. Letting us solving  $z^{k+1}$  with  $y^{k+1}$  first. By  $(\sigma_k I + \partial p^*)(z^{k+1}) \ni -\sigma \mathcal{V}_b^T y^{k+1} - \lambda^k$ , we now solve  $z^{k+1}$  from (3.15)

$$z^{k+1} = (I + \frac{1}{\sigma_k} \partial p^*)^{-1} (-\mathcal{V}_b^T y^{k+1} - \frac{\lambda^k}{\sigma_k}). \quad (3.17)$$

Substituting  $z^{k+1}$  in (3.17) into (3.14), we obtain

$$\nabla h^*(y^{k+1}) + \mathcal{V}_b \lambda^k + \sigma \mathcal{V}_b \mathcal{V}_b^T y^{k+1} + \sigma_k \mathcal{V}_b (I + \frac{1}{\sigma_k} \partial p^*)^{-1} (-\mathcal{V}_b^T y^{k+1} - \frac{\lambda^k}{\sigma_k}) \ni 0.$$

With Moreau's identity

$$x = (I + \sigma \partial G)^{-1}(x) + \sigma (I + \frac{1}{\sigma} \partial G^*)^{-1}(\frac{x}{\sigma}),$$

and by letting  $x = -\sigma_k \mathcal{V}_b^T y^{k+1} - \lambda^k$ , and  $G(x) = p(x)$ , we get  $\sigma_k z^{k+1}$  as follows

$$\sigma_k (I + \frac{1}{\sigma_k} \partial p^*)^{-1} (-\mathcal{V}_b^T y^{k+1} - \frac{\lambda^k}{\sigma_k}) = -\sigma_k \mathcal{V}_b^T y^{k+1} - \lambda^k - (I + \sigma_k \partial p)^{-1} (-\sigma_k \mathcal{V}_b^T y^{k+1} - \lambda^k). \quad (3.18)$$

Substituting the above formula which is  $\sigma_k z^{k+1}$  actually into (3.15), we arrive at

$$\nabla h^*(y^{k+1}) + \mathcal{V}_b \lambda^k + \sigma_k \mathcal{V}_b \mathcal{V}_b^T y^{k+1} + \mathcal{V}_b \underbrace{(-\sigma_k \mathcal{V}_b^T y^{k+1} - \lambda^k - (I + \sigma_k \partial p)^{-1} (-\sigma_k \mathcal{V}_b^T y^{k+1} - \lambda^k))}_{\sigma_k z^{k+1}} = 0.$$

This leads to the following nonlinear equation of  $y^{k+1}$  on  $L^2(\partial\Omega)$  finally

$$\partial h^*(y) - \mathcal{V}_b (I + \sigma \partial p)^{-1} (-\lambda^k - \sigma_k \mathcal{V}_b^T y) = 0. \quad (3.19)$$

Since  $\nabla h^*(y) = y + u_b$  with (3.7), the nonlinear equation (3.19) on  $y^{k+1}$  becomes

$$\mathcal{F}_k(y) = 0, \quad \mathcal{F}_k(y) := y + u_b - \mathcal{V}_b(I + \sigma_k \partial p)^{-1}(-\lambda^k - \sigma_k \mathcal{V}_b^T y) = 0. \quad (3.20)$$

Note that  $y \in L^2(\partial\Omega)$  and the nonlinear equation (3.20) is on the boundary  $\partial\Omega$ , which can be of much smaller scale compared to the source  $\mu$  to be reconstructed. Since  $(I + \sigma \partial p)^{-1}(\cdot)$  is a semismooth function for any positive  $\sigma$ , we have the following lemma for the semismooth Newton derivative of  $\mathcal{F}$ .

**Lemma 1.** *The semismooth Newton derivative of  $\mathcal{F}_k(y)$  is*

$$(\partial F_k(y))(z) = (I + \frac{\sigma_k}{1 + \sigma_k \alpha_0} \mathcal{V}_b \mathcal{X}_y^k \mathcal{V}_b^T)(z) \quad (3.21)$$

where  $\mathcal{X}_y^k$  can be chosen as follows

$$\mathcal{X}_y^k := \begin{cases} \{1\}, & |\lambda^k + \sigma_k \mathcal{V}_b^T y| > \sigma_k \alpha \\ \{0\}, & |\lambda^k + \sigma_k \mathcal{V}_b^T y| < \sigma_k \alpha \\ [0, 1], & |\lambda^k + \sigma_k \mathcal{V}_b^T y| = \sigma_k \alpha \end{cases} \quad (3.22)$$

*Proof.* For the resolvent  $(I + \sigma_k \partial p)^{-1}$  in (3.20), let us introduce

$$w := (I + \sigma_k \partial p)^{-1}(\mu) = \arg \min_{\tilde{w}} \frac{\|\tilde{w} - \mu\|_2^2}{2} + \frac{\sigma_k \alpha_0}{2} \|\tilde{w}\|_{L^2(\Omega)}^2 + \sigma_k \alpha \|\tilde{w}\|_{L^1(\Omega)}.$$

By the optimality condition, we have

$$0 \in w - \mu + \sigma_k \alpha_0 w + \sigma_k \alpha \partial \|w\|_1 \Leftrightarrow \mu \in (1 + \sigma_k \alpha_0)w + \sigma_k \alpha \partial \|w\|_1 \quad (3.23)$$

$$\Rightarrow w = (I + \frac{\sigma_k \alpha}{1 + \sigma_k \alpha_0} \partial \|\cdot\|_1)^{-1}(\frac{\mu}{1 + \sigma_k \alpha_0}) = \mathcal{S}_{\frac{\sigma_k \alpha}{1 + \sigma_k \alpha_0}}(\frac{\mu}{1 + \sigma_k \alpha_0}). \quad (3.24)$$

Now, introducing  $l(y) := (I + \sigma_k \partial p)^{-1}(-\lambda - \sigma_k \mathcal{V}_b^T y)$ , we can write its expression component-wisely

$$[l(y)]_i = \begin{cases} \frac{(-\lambda - \sigma_k \mathcal{V}_b^T y)_i}{1 + \sigma_k \alpha_0} - \frac{\sigma \alpha}{1 + \sigma_k \alpha_0}, & \text{if } (-\lambda - \sigma_k \mathcal{V}_b^T y)_i > \sigma_k \alpha, \\ 0, & \text{if } |(-\lambda - \sigma_k \mathcal{V}_b^T y)_i| \leq \sigma_k \alpha \\ \frac{(-\lambda - \sigma_k \mathcal{V}_b^T y)_i}{1 + \sigma_k \alpha_0} + \frac{\sigma \alpha}{1 + \sigma_k \alpha_0}, & \text{if } (-\lambda - \sigma_k \mathcal{V}_b^T y)_i < -\sigma_k \alpha. \end{cases} \quad (3.25)$$

It can be checked that  $l(y)$  is a  $PC^1$  function (piecewise differentiable function) [43, Proposition 4.3.1]. Since  $l(y)$  is continuous differentiable on  $y_i$  when  $|(-\lambda - \sigma_k \mathcal{V}_b^T y)_i| > \sigma_k \alpha$ , we have  $[(\partial l)(z)]_i = (-\frac{\sigma}{1 + \sigma_k \alpha_0} \mathcal{V}_b(z))_i$ . While  $|(-\lambda - \sigma_k \mathcal{V}_b^T y)_i| < \sigma_k \alpha$ , we obtain  $[(\partial l)(z)]_i = 0$ . For the case  $|(-\lambda - \sigma_k \mathcal{V}_b^T y)_i| = \sigma_k \alpha$ , by [43, Theorem 4.3.1], we have  $s(\frac{-\sigma_k}{1 + \sigma_k \alpha_0} \mathcal{V}_b(z))_i \in [(\partial l)(z)]_i$  for any  $s \in [0, 1]$ . Since the soft thresholding operator  $\mathcal{S}_{\frac{\sigma_k \alpha}{1 + \sigma_k \alpha_0}}$  is anisotropic on  $y$ . We finally arrive at the semismooth Newton derivative  $\partial F$  as in (3.21).  $\square$

The Newton update for solving  $y^{k+1}$  becomes that for  $l = 0, 2, \dots$ , with  $y^0 = y^k$

$$\mathcal{N}(y^l)(y^{l+1} - y^l) = -F(y^l), \quad \mathcal{N}(y^l) \in \partial F(y^l). \quad (3.26)$$

*Remark 1.* It can be seen that from (3.21), the semismooth Newton derivative is a positive definite and bounded operator. Thus for the Newton update in (3.26) and any  $\mathcal{N}(y^l) \in \partial F(y^l)$ , we have  $\mathcal{N}(y^l) \succ I$  and  $\mathcal{N}(y^l)^{-1}$  is uniformly bounded. The Newton update (3.26) is well-defined.

After obtaining  $y^{l+1}$ , we can calculate  $z^{k+1}$  by (3.18) as follows

$$z^{l+1} = \mathcal{M}^k(y^{l+1}), \quad \mathcal{M}^k(y^{l+1}) := \frac{1}{\sigma_k}[-\sigma_k \mathcal{V}_b^T y^{l+1} - \lambda^k - (I + \sigma_k \partial p)^{-1}(-\sigma_k \mathcal{V}_b^T y^{l+1} - \lambda^k)]. \quad (3.27)$$

Since Newton methods, including semismooth Newton methods, are always locally convergent. Line search is usually employed for globalization and convergence. We use the following Armijo line search strategy. By defining  $d^l = y^{l+1} - y^l$ , we proceed with an *aggressive* Armijo-type line search involving parameters  $\beta^t > 0$ ,  $t = 0, 1, 2, \dots$ ,  $\beta \in (0, 1)$ , and  $c > 0$ . The objective is to find the smallest integer  $t$  satisfying:

$$L_{\sigma_k}(y^l + \beta^t d^l, \mathcal{M}^k(y^l + \beta^t d^l); \lambda^k) \leq L_{\sigma_k}(y^l, \mathcal{M}^k(y^l); \lambda^k) - c\beta^t \|d^l\|_2^2. \quad (3.28)$$

The final step size  $t_l := \beta^t$  obtained from the line search in (3.28) dictates the update of  $y^{k+1}$  as follows:

$$y^{l+1} = y^l + t_l d^l. \quad (3.29)$$

Once some stopping criterion for inner Newton iteration is satisfied, e.g., for some  $l = l_0$ , we set  $y^{k+1} = y^{l_0}$  and obtain  $z^{k+1}$  with  $z^{k+1} = \mathcal{M}^k(y^{k+1})$ . After finishing the inner semismooth Newton iterations, we then update  $\lambda^{k+1}$  as in (3.14b) for the outer ALM updates. Once the stopping criterion of the outer ALM iterations is satisfied with  $(y^K, z^K, \lambda^K)$ , the solution  $\mu$  corresponding to the primal problem can be approximated by

$$\mu^K = (I + \frac{\alpha}{\alpha_0} \partial \|\cdot\|_1)^{-1} \left( \frac{-\mathcal{V}_b^T y^K}{\alpha_0} \right), \quad (3.30)$$

which has an explicit solution. Since by the primal-dual optimality conditions of (3.10) at saddle-points  $(y^*, \mu^*)$ , we have

$$-\mathcal{V}_b^T y^* \in \partial p(\mu^*) \Leftrightarrow -\mathcal{V}_b^T y^* \in \alpha \partial \|\cdot\|_1 + \alpha_0 \mu^* \Leftrightarrow \mu^* = (I + \frac{\alpha}{\alpha_0} \partial \|\cdot\|_1)^{-1} \left( \frac{-\mathcal{V}_b^T y^*}{\alpha_0} \right).$$

Finally, let us conclude this section with the proposed semismooth Newton-based ALM as the following Algorithm 1. We then discuss its convergence in the next section.

---

**Algorithm 1** Boundary measurements based dual Augmented Lagrangian method with semismooth Newton solver for (2.8) (ALM-bd-SSN)

---

**Require:** Given linear operator  $\mathcal{V}_b$  and  $u_b$ , regularization parameters  $(\alpha_0, \alpha)$ , and parameter settings for ALM  $\sigma_0, c_0, \beta, \rho$ , and initial vectors  $(y_0, z_0, \lambda_0)$ ,  
 set  $y = y_0, \sigma = \sigma_0, \lambda = \lambda_0$   
**while**  $0 \leq i \leq K_{\max}$  and some stopping criterion for outer ALM iterations is satisfied  
**do**  
**while**  $l \leq L$  and some stopping criterion for inner SSN is satisfied **do**  
 Calculate  $\mathcal{X}_y^k$  in (3.22) and Newton derivative (3.21), and solve (3.26) for SSN update.  
 Do Armijo line search (3.28) and update  $y^{l+1}$  with (3.29).  
**end while**  
 Compute  $z^{k+1} = \mathcal{M}^k(y^{k+1})$  by (3.27).  
 Update  $\lambda^{k+1}$  by (3.14b).  
 Update  $\sigma_{k+1} = c_0 \sigma_k$ .  
**end while**  
 Obtain the reconstructed  $\mu$  with (3.30) finally.

---

### 3.2 Convergence of the SSN-based ALM on the dual space

Now we introduce some basic definitions and properties of multivalued mapping from convex analysis [20, 37]. Let  $F : X \rightrightarrows Y$  be a multivalued mapping. The graph of  $F$  is defined as the set

$$\text{gph}F := \{(x, y) \in X \times Y \mid y \in F(x)\}.$$

The inverse of  $F$ , i.e.,  $F^{-1} : Y \rightrightarrows X$  is defined as the multivalued mapping whose graph is  $\{(y, x) \mid (x, y) \in \text{gph}F\}$ . The distance  $x$  from the set  $C \subset X$  is defined by

$$\text{dist}(x, C) := \inf\{\|x - x'\| \mid x' \in C\}.$$

For the local convergence rate of ALM, we need the metrical subregularity [20].

**Definition 1** (Metric Subregularity [20]). A mapping  $F : X \rightrightarrows Y$  is called metrically subregular at  $\bar{x}$  for  $\bar{y}$  if  $(\bar{x}, \bar{y}) \in \text{gph}F$  and there exists modulus  $\kappa \geq 0$  along with a neighborhoods  $U$  of  $\bar{x}$  and  $V$  of  $\bar{y}$  such that

$$\text{dist}(x, F^{-1}(\bar{y})) \leq \kappa \text{dist}(\bar{y}, F(x) \cap V) \quad \text{for all } x \in U. \quad (3.31)$$

Now, let us turn to the primal problem (3.1), which is the dual problem (3.10). For the  $L^1$  norm, we see

$$\|\mu\|_1 = \sum_{i=1}^M |\mu_i| \quad (3.32)$$

which is a polyhedral function. Introduce the Lagrangian function

$$l(y, z, \lambda) = p^*(z) + h^*(y) + \langle \lambda, \mathcal{V}_b^* y + z \rangle_{L^2(\Omega)}. \quad (3.33)$$

It is well-known that  $l$  is a convex-concave function on  $(u, p, \lambda)$ . Define the maximal monotone operator  $T_l$  by

$$T_l(y, z, \lambda) = \{(y', z', \lambda') | (y', z', -\lambda') \in \partial l(y, z, \lambda)\}, \quad (3.34)$$

and the corresponding inverse is given by

$$T_l^{-1}(y', z', \lambda') = \{(y, z, \lambda) | (y', z', -\lambda') \in \partial l(y, z, \lambda)\}. \quad (3.35)$$

Here, adding the negative sign as in  $-\lambda'$  is because  $l$  is concave on  $\lambda$ .

**Theorem 2.** *For the dual problem (3.10), assuming the KKT system has at least one solution, then  $T_l$  is metrically subregular at  $(y^*, z^*, \lambda^*)^T$  for the origin. Similarly, assuming  $(\partial\mathcal{P})^{-1}(0) \neq \emptyset$  as  $\mathcal{P}$  in (3.1),  $\partial\mathcal{P}$  are metrically subregular at  $\lambda^*$  for the origin.*

*Proof.* With direct calculation, we have

$$T_l(y, z, \lambda) = (\partial h^*(y) + \mathcal{V}_b \lambda, \partial p^*(z) + \lambda, -z - \mathcal{V}_b^T y)^T := \mathcal{A}(x) + \mathcal{B}(x),$$

where

$$\mathcal{A} \begin{pmatrix} y \\ z \\ \lambda \end{pmatrix} := \begin{pmatrix} \partial h^* & 0 & 0 \\ 0 & \partial p^* & 0 \\ 0 & 0 & 0 \end{pmatrix} \begin{pmatrix} y \\ z \\ \lambda \end{pmatrix}, \quad \mathcal{B} \begin{pmatrix} y \\ z \\ \lambda \end{pmatrix} := \begin{pmatrix} 0 & 0 & \mathcal{V}_b \\ 0 & 0 & I \\ -\mathcal{V}_b^T & -I & 0 \end{pmatrix} \begin{pmatrix} y \\ z \\ \lambda \end{pmatrix}. \quad (3.36)$$

It is known that the  $\|\cdot\|_1$  (3.32) is a polyhedral convex function. We can see that  $\partial h^*$  is a polyhedral function of  $y$  and  $\partial p^*$  is a polyhedral function of  $z$ . We thus conclude that the monotone operator  $\mathcal{A}$  is polyhedral. Besides, the operator  $\mathcal{B}$  is a maximal monotone and linear operator. Thus  $T_l$  is a polyhedral mapping [40]. By the corollary in [40], we see  $T_l$  is metrically subregular at  $(y^*, z^*, \lambda^*)^T$  for the origin.

Let us now turn to the metric subregularity of  $\partial\mathcal{P}$ , which is a dual function of the dual problem (3.10). Supposing  $(\partial\mathcal{P})^{-1}(0) \neq \emptyset$ , since

$$(\partial\mathcal{P})(\mu) = \mathcal{V}_b^T(\mathcal{V}_b \mu - u_b) + \alpha_0 \mu + \alpha \partial\|\mu\|_1. \quad (3.37)$$

We conclude that it is a polyhedral mapping of  $\mu$ . With the corollary in [40],  $\partial\mathcal{P}$  is metrically subregular.  $\square$

Here, we follow the standard stopping criterion for the inexact augmented Lagrangian method originated [41, 42].

$$L_{\sigma^k}(y^{k+1}, z^{k+1}; \lambda^k) - \inf_{y, z} L_{\sigma^k}(y, z; \lambda^k) \leq \epsilon_k^2 / (2\sigma_k), \quad \sum_{k=0}^{\infty} \epsilon_k < \infty, \quad (\text{A})$$

$$L_{\sigma^k}(y^{k+1}, z^{k+1}; \lambda^k) - \inf_{y, z} L_{\sigma^k}(y, z; \lambda^k) \leq (\delta_k^2 / (2\sigma_k)) \|\lambda^{k+1} - \lambda^k\|^2, \quad \sum_{k=0}^{\infty} \delta_k < +\infty, \quad (\text{B1})$$

$$\text{dist}(0, \partial L_{\sigma^k}(y, z; \lambda^k)|_{y, z}) \leq (\delta_k' / \sigma_k) \|\lambda^{k+1} - \lambda^k\|, \quad 0 \leq \delta_k' \rightarrow 0. \quad (\text{B2})$$

Before discussing the local convergence rate, let us turn to the relation between  $\mu$  and the Lagrangian multiplier  $\lambda$ . It is known that the saddle-points of the augmented Lagrangian functional (3.12) and the Lagrangian functional (3.33) are the same. Let us focus on (3.33). With direct calculation, we have

$$\inf_{y, z} \sup_{\lambda} l(y, z, \lambda) = p^*(z) + h^*(y) + \langle \mathcal{V}_b^T y + z, \lambda \rangle \Leftrightarrow \quad (3.38)$$

$$\sup_{\lambda} -[\sup_y \langle y, -\mathcal{V}_b \lambda \rangle - h^*(y) + \sup_z \langle -\lambda, z \rangle - p^*(z)] \Leftrightarrow \quad (3.39)$$

$$\sup_{\lambda} -(h(-\mathcal{V}_b \lambda) + p(-\lambda)) \Leftrightarrow -\inf_{\lambda} (h(-\mathcal{V}_b \lambda) + p(-\lambda)). \quad (3.40)$$

Compared to (3.6), we conclude that optimal solutions  $\mu^*$  of (3.6) and  $\lambda^*$  of (3.40) have the relation  $\mu^* = -\lambda^*$ . The convergence of  $\mu^k$  is dominated by  $\lambda^k$ . We can also obtain the convergence rate of  $\mu^k$  from the convergence rate of  $y^k$  by (3.30). Since  $(I + \frac{\alpha}{\alpha_0} \partial \|\cdot\|_1)^{-1}$  is a firmly nonexpansive operator, we have

$$\|\mu^k - \mu^{k+1}\| \leq c_0 \|y^k - y^{k+1}\|, \quad \|\mu^k - \mu^*\| \leq c_0 \|y^k - y^*\|, \quad c_0 := \|\mathcal{V}_b^T\| / \alpha_0.$$

Henceforth, we only focus on the convergence rate of  $(y^k, z^k, \lambda^k)$ .

We denote  $\mathcal{X}^P$  as the solution sets of the problem (3.1). With these preparations, we have the following global convergence and local convergence rate for the ALM method (3.14), under the mild condition that the KKT system of (3.33) has at least one solution, as in Theorem 2.

**Theorem 3.** *For the dual problem (3.10) and corresponding ALM (3.14), denote the iteration sequence  $(y^k, z^k, \lambda^k)$  generated by ALM-bd-SSN with stopping criteria (A). The sequence  $(y^k, z^k, \lambda^k)$  is bounded and converges to  $(y^*, z^*, \lambda^*)$  globally.  $T_d = \partial \mathcal{P}$  is metrically subregular for the origin with modulus  $\kappa_d$  and with the additional stopping criteria (B1), the sequence  $\{\lambda^k\}_k$  converges to  $\lambda^* \in \mathcal{X}^P$ . For sufficiently large  $k$ , we have the following local linear convergence*

$$\text{dist}(\lambda^{k+1}, \mathcal{X}^P) \leq \theta_k \text{dist}(\lambda^k, \mathcal{X}^P), \quad (3.41)$$

where

$$\theta_k = [\kappa_d(\kappa_d^2 + \sigma_k^2)^{-1/2} + \delta_k](1 - \delta_k)^{-1}, \text{ as } k \rightarrow \infty, \theta_k \rightarrow \theta_\infty = \kappa_d(\kappa_d^2 + \sigma_\infty^2)^{-1/2} < 1.$$

Furthermore,  $T_l$  is metrically subregular at  $(y^*, z^*, \lambda^*)$  for the origin with modulus  $\kappa_l$ . When the additional stopping criteria (B2) is employed, for sufficiently large  $k$ , we have

$$\|(y^{k+1}, z^{k+1}) - (y^k, z^k)\| \leq \theta'_k \|\lambda^{k+1} - \lambda^k\|, \quad (3.42)$$

where  $\theta'_k = \kappa_l(1 + \delta'_k)/\sigma_k$  with  $\lim_{k \rightarrow \infty} \theta'_k = \kappa_l/\sigma_\infty$ .

*Proof.* Since discrete  $L^2(\partial\Omega)$  is a finite-dimensional reflexive space and the dual function (3.10) is lower semicontinuous, proper, and strongly convex due to the strong convexity of  $h^*$ , it is coercive. Thus, the existence of the solution can be guaranteed [28, Theorem 4.25]. Furthermore, since  $\text{dom } \mathcal{D} = L^2(\partial\Omega)$ , by Fenchel-Rockafellar theory [28, Chapter 4.3], the solution to the dual problem (3.10) is not empty and  $\min_\mu \mathcal{P}(\mu) = \max_y -\mathcal{D}(y)$ . By [42, Theorem 4] (or [41, Theorem 1] where the augmented Lagrangian method (3.14) essentially comes from proximal point method applying to its dual problem, i.e., the primal problem (3.1)), with criterion (A), we get the boundedness of  $\{\lambda^k\}_k$ . The uniqueness of  $(y^*, z^*)$  follows from the strong convexity of  $h^*$  on  $y$  and the  $z^* = -\mathcal{V}_b^T y^*$ , which is one of the KKT conditions. The boundedness of  $(y^k, z^k)$  and convergence of  $(y^k, z^k, \lambda^k)$  then follows by [42, Theorem 4].

By Theorem 2, we have metrical subregularity of  $T_d = \partial\mathcal{P}$ . With the stopping criteria (A) and (B1), the local convergence rate (3.41) can thus be obtained from [42, Theorem 5] (or [41, Theorem 2]). Now we turn to the local convergence rate of  $(y^k, z^k)$ . By the metrical subregularity of  $T_l$  as in Theorem 2, for sufficiently large  $k$ , we have

$$\|(y^{k+1}, z^{k+1}) - (y^*, z^*)\| + \text{dist}(\lambda^k, \mathcal{X}^P) \leq \kappa_l \text{dist}(0, T_l(y^{k+1}, z^{k+1}, \lambda^{k+1})).$$

Together with the stopping criteria (B2) and [42] (Theorem 5 and Corollary in Section 4), we arrive at

$$\begin{aligned} \|(y^{k+1}, z^{k+1}) - (y^*, z^*)\| &\leq \kappa_l \sqrt{\delta_k'^2 \sigma_k^{-2} \|\lambda^{k+1} - \lambda^k\|^2 + \sigma_k^{-2} \|\lambda^{k+1} - \lambda^k\|^2} \\ &= \kappa_l \sqrt{\delta_k'^2 + 1} \sigma_k^{-1} \|\lambda^{k+1} - \lambda^k\| \leq \theta'_k \|\lambda^{k+1} - \lambda^k\|, \end{aligned}$$

which leads to (3.42). □

## 4 Semismooth Newton Method and First-Order Primal-dual Method

In this section, we will introduce a semismooth Newton method and a first-order primal-dual method for the inverse source scattering problem. Let us first discuss the semismooth

Newton method. For the primal formulation (3.1), if choosing

$$f(z) := \frac{1}{2} \langle B^{-1}z, z \rangle_{L^2(\Omega)} - \langle z, B^{-1}\mathcal{V}_b^T u_b \rangle_{L^2(\Omega)} + d_0, \quad g(z) := \alpha \|z\|_{L^1(\Omega)}, \quad (4.1)$$

where  $B := \mathcal{V}_b^T \mathcal{V}_b + \alpha_0 I$ . The the primal formulation can be written as  $\min_{\mu} f(B\mu) + g(\mu)$ . By the Fenchel–Rockafellar duality, the predual problem is  $\min_y f^*(y) + g^*(-B^T y)$ , which is

$$\begin{aligned} \min_y & \langle y, By + \mathcal{V}_b^T u_b \rangle_{L^2(\Omega)} - \frac{1}{2} \langle y + B^{-1}\mathcal{V}_b^T u_b, By + \mathcal{V}_b^T u_b \rangle_{L^2(\Omega)} + \langle y + B^{-1}\mathcal{V}_b^T u_b, \mathcal{V}_b^T u_b \rangle_{L^2(\Omega)} \\ & - d_0 + \mathcal{I}_{\{\|B^T y\|_{\infty} \leq \alpha\}}(y) \end{aligned} \quad (4.2)$$

We then use Moreau–Yosida regularization for dealing with the constraint  $\|B^T y\|_{\infty} \leq \alpha$  as follows

$$\begin{aligned} \min_y & E(y), \quad E(y) := \langle y, By + \mathcal{V}_b^T u_b \rangle_{L^2(\Omega)} - \frac{1}{2} \langle y + B^{-1}\mathcal{V}_b^T u_b, Bz + \mathcal{V}_b^T u_b \rangle_{L^2(\Omega)} \\ & + \langle y + B^{-1}\mathcal{V}_b^T u_b, \mathcal{V}_b^T u_b \rangle_{L^2(\Omega)} - d_0 + \frac{1}{2\gamma} \|\max(0, \gamma(B^T y - \alpha))\|_2^2 + \frac{1}{2\gamma} \|\min(0, \gamma(B^T y + \alpha))\|_2^2. \end{aligned} \quad (4.3)$$

Although there is  $B^{-1}$  in the above functional (4.3), with direct calculation by the first-order optimality condition of the functional (4.3), no  $B^{-1}$  is involved in the following nonlinear equation, fortunately,

$$F(y) = \nabla E(y) = By + \mathcal{V}_b^T u_b + \gamma B \max(0, B^T y - \alpha) + \gamma B \min(0, B^T y + \alpha) = 0. \quad (4.4)$$

The formulation  $\max(0, B^T y - \alpha)$  or  $\min(0, B^T y + \alpha)$  is understood in point-wise sense. For their subgradients, we introduce  $\mathcal{A}_k^+ = \{x \in \Omega : B^T y^k(x) \geq \alpha\}$ ,  $\mathcal{A}_k^- = \{x \in \Omega : B^T y^k(x) \leq -\alpha\}$ , and  $\mathcal{A}_k = \mathcal{A}_k^+ \cup \mathcal{A}_k^-$  along with  $\chi_{\mathcal{A}^+} = \text{Diag}([\chi_{\mathcal{A}^+}]_1, [\chi_{\mathcal{A}^+}]_2, \dots)$ ,  $\chi_{\mathcal{A}^-} = \text{Diag}([\chi_{\mathcal{A}^-}]_1, [\chi_{\mathcal{A}^-}]_2, \dots)$  and  $\chi_{\mathcal{A}} = \text{Diag}([\chi_{\mathcal{A}}]_1, [\chi_{\mathcal{A}}]_2, \dots)$  depend on  $y$  and their diagonal elements are defined by

$$[\chi_{\mathcal{A}^+}]_i = \begin{cases} 1, & [B^T y^k]_i \geq \beta, \\ 0, & [B^T y^k]_i < \beta, \end{cases} \quad [\chi_{\mathcal{A}^-}]_i = \begin{cases} 1, & [B^T y^k]_i \leq -\beta, \\ 0, & [B^T y^k]_i > -\beta, \end{cases} \quad [\chi_{\mathcal{A}}]_i = [\chi_{\mathcal{A}^+}]_i + [\chi_{\mathcal{A}^-}]_i. \quad (4.5)$$

With these preparations, the semismooth Newton method for solving the nonlinear system  $F(y) = 0$  reads as

$$\mathcal{N}(y^k)y^{k+1} = \mathcal{N}(y^k)y^k - F(y^k), \quad (4.6)$$

where  $B + \gamma B \mathcal{X}_{\mathcal{A}_k} B^T = \mathcal{N}(y^k) \in \partial F(y^k)$ , so we get

$$(B + \gamma B \mathcal{X}_{\mathcal{A}_k} B^T)y^{k+1} = -\mathcal{V}_b^T u_b + \gamma \alpha B(\mathcal{X}_{\mathcal{A}_k^+} - \mathcal{X}_{\mathcal{A}_k^-})\vec{1}. \quad (4.7)$$

We let  $\gamma \rightarrow \infty$  with path-following strategy [25] (or [28, Section 9.1]). Finally, we can recover  $\mu$  with  $y$  by (3.5)

$$B\mu^* = \nabla f^*(y) \rightarrow \mu = B^{-1}\nabla f^*(y^*) = y^* + B^{-1}(\mathcal{V}_b^T u_b). \quad (4.8)$$

We conclude the above discussions with the following semismooth Newton algorithm, i.e., Algorithm 2.

---

**Algorithm 2** Semismooth Newton method (shortened as SSN)

---

**Require:**  $y^0 \in L^2(\Omega)$ , strictly increasing path-following parameters  $[\gamma_0, \gamma_1, \dots, \gamma_{K_{\max}}]$ , with  $\gamma_i > 0$   $i = 1, \dots, K_{\max}$ .

**Ensure:**  $y, \mu$

- 1: Initialization  $y_{\gamma_0}^0 = y^0$
- 2: **while**  $0 \leq i \leq I, \gamma = \gamma_i$  **do**
- 3:   **while**  $k \leq K$  **do**
- 4:     Calculate active sets and the corresponding functions as in (4.5) for  $\gamma = \gamma_i$ .
- 5:     Solve for  $y^k \in L^2(\Omega)$  by (4.7) and denote it  $y_{\gamma_i}^k$ .
- 6:     Update  $\mathcal{A}_k^+, \mathcal{A}_k^-, \mathcal{A}_k$
- 7:     Until  $\mathcal{A}_k^+ = \mathcal{A}_{k-1}^+, \mathcal{A}_k^- = \mathcal{A}_{k-1}^-$ , set  $y_{\gamma_{i+1}}^0 = y_{\gamma_i}^k$ .
- 8:   **end while**
- 9: **end while**
- 10:  $y = y_{\gamma_{K_{\max}}}^k$
- 11:  $\mu = B^{-1}\nabla f^*(y) = y + B^{-1}(\mathcal{V}_b^T u_b)$ .

---

## 4.1 First-order primal-dual method

Finally, let us turn to the first-order methods. The Chambolle-Pock's first-order primal-dual algorithm [14] is employed and studied for the inverse medium scattering problem in [12, 13]. Here, for comparison, we also presented the first-order primal-dual algorithm. With

$$\frac{1}{2}\|\mathcal{V}_b\mu - u_b\|_{L^2(\partial\Omega)}^2 = \max_{p \in L^2(\partial\Omega)} \langle \mathcal{V}_b\mu - u_b, p \rangle_{L^2(\partial\Omega)} - \frac{1}{2}\|p\|_{L^2(\partial\Omega)}^2,$$

we get the following primal-dual problem

$$\min_{\mu} \max_p \langle \mathcal{V}_b\mu - u_b, p \rangle_{L^2(\partial\Omega)} - \frac{1}{2}\|p\|_{L^2(\partial\Omega)}^2 + \frac{\alpha_0}{2}\|\mu\|_{L^2(\Omega)}^2 + \alpha\|\mu\|_{L^1(\Omega)} \Leftrightarrow \quad (4.9)$$

$$\min_{\mu} \max_p \langle \mathcal{V}_b\mu, p \rangle_{L^2(\partial\Omega)} + \frac{\alpha_0}{2}\|\mu\|_{L^2(\Omega)}^2 + \alpha\|\mu\|_{L^1(\Omega)} - \left( \frac{1}{2}\|p\|_{L^2(\partial\Omega)}^2 + \langle u_b, p \rangle_{L^2(\partial\Omega)}^2 \right). \quad (4.10)$$

Setting  $F^*(p) = \frac{1}{2}\|p\|_{L^2(\partial\Omega)}^2 + \langle u_b, p \rangle_{L^2(\partial\Omega)}$  and  $G(\mu) = \frac{\alpha_0}{2}\|\mu\|_{L^2(\Omega)}^2 + \alpha\|\mu\|_{L^1(\Omega)}$ , we have

$$(I + \sigma\partial F^*)^{-1}(\bar{p}) = \frac{\bar{p} - \sigma u_b}{1 + \sigma}, \quad (I + \tau\partial G)^{-1}(\bar{\mu}) = \text{sign}(\bar{\mu}) \max \left\{ \frac{|\bar{\mu}| - \tau\alpha}{1 + \tau\alpha_0}, 0 \right\}.$$

We now can employ the first-order primal-dual algorithm [14, Algorithm 1] to solve (2.8) with saddle-point formulation (4.10), as the following Algorithm 3.

---

**Algorithm 3** First-order primal-dual algorithm (PDA)

---

**Require:** initial vectors  $(p_0, \mu_0) \in L^2(\partial\Omega) \times L^2(\Omega)$ , step sizes  $(\sigma, \tau)$ ,  
**Ensure:**  $p, \mu$

- 1: set  $p = p_0, \mu = \mu_0, \bar{\mu} = \mu_0$
- 2: **for**  $0 \leq k \leq K_{\max}$  **do**
- 3:  $p_{k+1} = (I + \sigma \partial F^*)^{-1}(p_k + \sigma \mathcal{V}_b \bar{\mu}_k) = \frac{p_k + \sigma \mathcal{V}_b \bar{\mu}_k - \sigma u_b}{1 + \sigma}$
- 4:  $\mu_{k+1} = (I + \tau \partial G)^{-1}(\mu_k - \tau \mathcal{V}_b^T p_{k+1}) = \text{sign}(\mu_k - \tau \mathcal{V}_b^T p_{k+1}) \max \left\{ \frac{|\mu_k - \tau \mathcal{V}_b^T p_{k+1}| - \tau \alpha}{1 + \tau \alpha_0}, 0 \right\}$
- 5:  $\bar{\mu}_{k+1} = \mu_{k+1} + \theta(\mu_{k+1} - \mu_k)$
- 6: **end for**

---

## 5 Numerical Experiments

In this section, we will first give a brief discussion of the discretization of the Lippmann-Schwinger volume potential, followed by the presentation of the numerical examples. We will first give the linear mapping from the acoustic source  $\mu$  to the boundary measurement  $u_b^s$  for the inhomogeneous medium. Since we have

$$-\Delta u^s - k^2 n(x) u^s = \mu \Rightarrow -\Delta u^s - k^2 u^s = k^2 \left( \frac{1}{k^2} \mu + (n-1) u^s \right), \quad (5.1)$$

which leads to the following Lippmann-Schwinger integral equation

$$u^s = \mathcal{V}_k \left( \frac{1}{k^2} \mu + (n(x) - 1) u^s \right). \quad (5.2)$$

Now let us introduce  $q(x) = n(x) - 1$  and

$$\mathcal{V}_k h := k^2 \int_{\Omega} \Phi(x, y) h(y) dy.$$

We have

$$u^s(x) = \frac{1}{k^2} (I - \mathcal{V}_k q)^{-1} \mathcal{V}_k \mu. \quad (5.3)$$

Substituting (5.3) into (5.2), we have

$$u^s(x) = \frac{1}{k^2} \mathcal{V}_k (I + q(I - \mathcal{V}_k q)^{-1} \mathcal{V}_k) \mu. \quad (5.4)$$

We finally obtain the linear mapping from the source  $\mu$  to the measurement

$$u_b^s(x) = T_r \circ \left[ \frac{1}{k^2} \mathcal{V}_k (I + q(I - \mathcal{V}_k q)^{-1} \mathcal{V}_k) \right] \mu, \quad T_r u := u|_{\partial\Omega}, \quad (5.5)$$

where  $T_r$  denotes the trace mapping. The source to measurement mapping can be

$$\mathcal{T} := T_r \circ \left[ \frac{1}{k^2} \mathcal{V}_k (I + q(I - \mathcal{V}_k q)^{-1} \mathcal{V}_k) \right] : \mathcal{M}(\Omega) \rightarrow T_r(W^{1,p}(\partial\Omega)). \quad (5.6)$$

The volume potential  $\mathcal{V}_k$  and  $(I - \mathcal{V}_k q)^{-1}$  can be computed by the Fourier-based collocation method by periodization of the Lippmann-Schwinger volume potential [31]. We adapted the code developed in [12, 13] where the discretization of  $\mathcal{T}$  is given, and we refer to [12, 13] for more details.

All algorithms are conducted with MATLAB R2024b on a Ubuntu 24.04 workstation with dual Intel (R) Xeon (R) E5-2697AV4 CPUs, 2.60 GHz, and 288 GB memory. The parameters of the compared algorithms are as follows

- ALM: ALM-bd-SSN as in Algorithm 1. We choose  $\sigma_0 = 1$  and  $\sigma_{k+1} = 6\sigma_k$ . For the Armijo line search, we choose  $\beta = 0.3$  and  $c = 10^{-4}$  as in (3.28).
- SSN: SSN as Algorithm 2. We choose  $\gamma_0 = 1$  and  $\gamma^i = 10^i$ ,  $i = 1, \dots, 8$ .
- PDA: First-order primal-dual algorithm as in Algorithm 3 [14]. We choose  $\sigma = 0.5$ ,  $\tau = 1/(\|\mathcal{V}_b^2\| + 10^{-6})\sigma$ , and  $\theta \equiv 1$ .

The Gaussian noise is added to get noisy boundary measurement  $u_b^\delta$  for the simulated data  $u$ , which is essentially as the same in [12, (73)]

$$(u_b^\delta - u_b)/\|u_b\|_2 = \delta(N_{\text{re}} + iN_{\text{im}})$$

where  $N_{\text{re}}$  and  $N_{\text{im}}$  are two real matrices sampled from standard normal distribution. We measure the reconstruction error by the following relative error

$$\text{N-Error} := \|\mu^{K_{\max}} - \mu_{\text{exa}}\|_2 / \|\mu_{\text{exa}}\|_2,$$

where  $\mu_{\text{exa}}$  is the exact acoustic source and  $K_{\max}$  is the corresponding maximum outer iteration number, and it varies for different algorithms.

To avoid “inverse crime”, we employ the code of [12, 13]. The strategy is that the discretization, especially the grid size of generating the synthetic data of the direct problem, is different from the discretization for reconstructing the unknown sources [12] (see also [47, Chapter 2.3.6]).

For the homogeneous medium, we choose the velocity  $c \equiv 1$  both in  $\mathbb{R}^2$  and  $\mathbb{R}^3$ . For the inhomogeneous medium, we employ the inhomogeneous medium from [26]

$$q(x) = \chi(x - \mathbf{0}), \quad \chi(t) = \begin{cases} \exp\left(\frac{-1}{1-|t|^2}\right) & |t| \leq 1, \\ 0 & |t| > 1, \end{cases} \quad (5.7)$$

where  $\mathbf{0} = (0, 0)^T$  in  $\mathbb{R}^2$  and  $\mathbf{0} = (0, 0, 0)^T$  in  $\mathbb{R}^3$ .

We computed the primal solution  $\mu^{K_{\max}}$  by (3.30) except the numerical examples in Figures 6 and 7, which are computed by  $-\lambda^{K_{\max}}$  due to (3.40) and the explanations there.

Now, let us turn to the numerical examples.

Figures 2 and 3 present the reconstructions of different point sources with %1 relative Gaussian noise error for homogeneous and inhomogeneous medium correspondingly. Table 1 collects the running time and relative errors of three different algorithms. For our experiments, we did not see big differences in running time between the homogeneous and the inhomogeneous medium. We thus only present the running time for the homogeneous case.

Figures 4 and 5 present the reconstructions of different strip sources with %0.1 relative Gaussian noise error for homogeneous and inhomogeneous medium correspondingly. Table 2 collects corresponding running time only for the homogeneous cases (still because the running time for the inhomogeneous cases is nearly the same as the homogeneous cases), relative errors for differential algorithms regarding homogeneous or inhomogeneous medium.

Figures 6 and 7 present the reconstructions of different 3-dimensional sources with %1 relative Gaussian noise error for homogeneous and inhomogeneous medium, respectively. Table 3 collects the running time and relative errors of ALM and SSN. It can be seen that the ALM can be 10 times faster than SSN. We did not compare with PDA since we found PDA is too slow. We computed the solution with  $-\lambda^k$  since  $\mu^* = -\lambda^*$  by (3.40) and numerically we found that  $\|\mu^{K_{\max}} + \lambda^{K_{\max}}\|$  is generally less than  $10^{-5}$  as  $K_{\max}$  being the maximal outer iteration number and  $\mu^{K_{\max}}$  computed by (3.30).

Figures 8 and 9 present the reconstructions of different 3-dimensional sources with %0.01 relative Gaussian noise error for homogeneous and inhomogeneous medium, correspondingly. Table 4 collects relative errors of ALM and SSN. Since the running time is similar to the %1 relative Gaussian noise error case, we omit the running time in Table 4.

## 6 Conclusions

We proposed a semismooth Newton-based augmented Lagrangian method on the “adjoint” space of measurement. The reconstruction can be greatly accelerated if the dimensions of the measurement data are much less than the unknown acoustic sources, which can be more than 10 times faster, as shown in the 3-dimensional numerical examples. It would be interesting to incorporate the multifrequency scattering data as was done in [3, 5, 6, 23]. We believe this framework can also benefit inverse medium problems and inverse electromagnetic wave scattering problems.

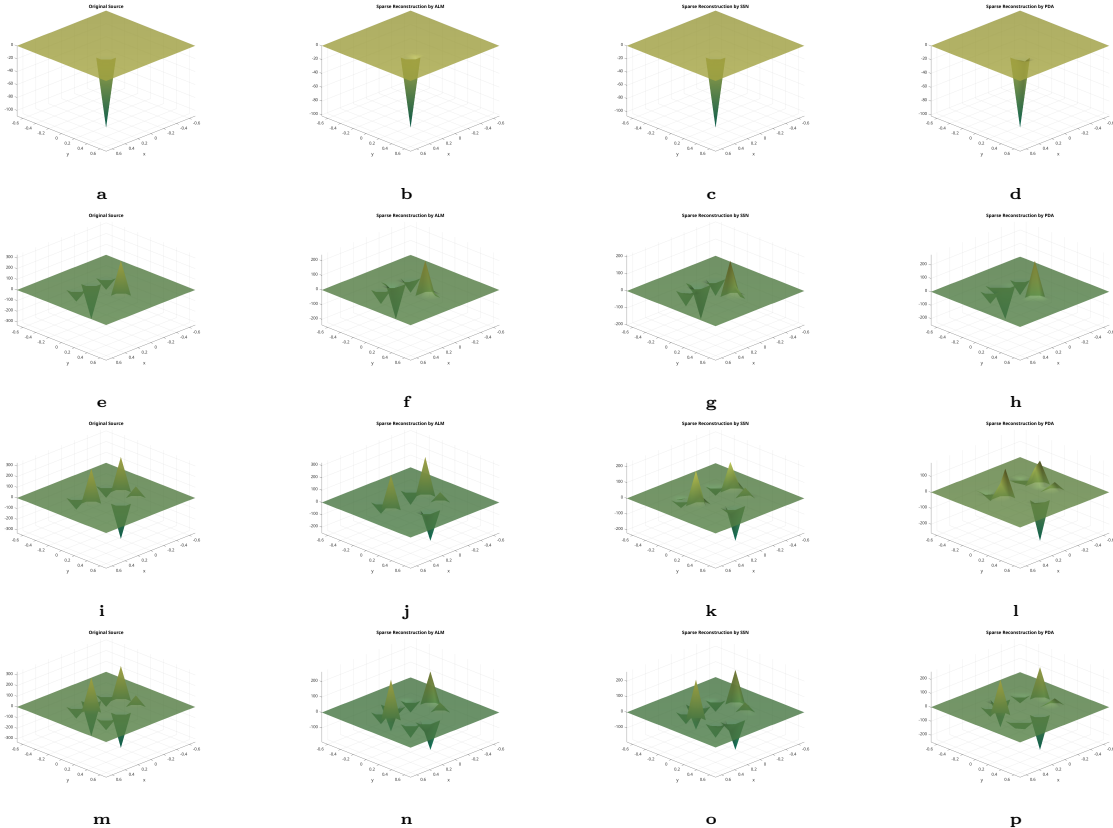


**Figure 2:** Reconstruction of sparse sources with multiple peaks in homogeneous media with  $k = 6$ . The figures in the leftmost column are the original acoustic sources, including one, four, six, and eight peaks. The images in the second, the third from the left, and the rightmost columns are reconstructed results of ALM, SSN, and PDA, respectively. The images in the first, second, third, and fourth rows are the sources with one, four, six, and eight peaks, respectively.

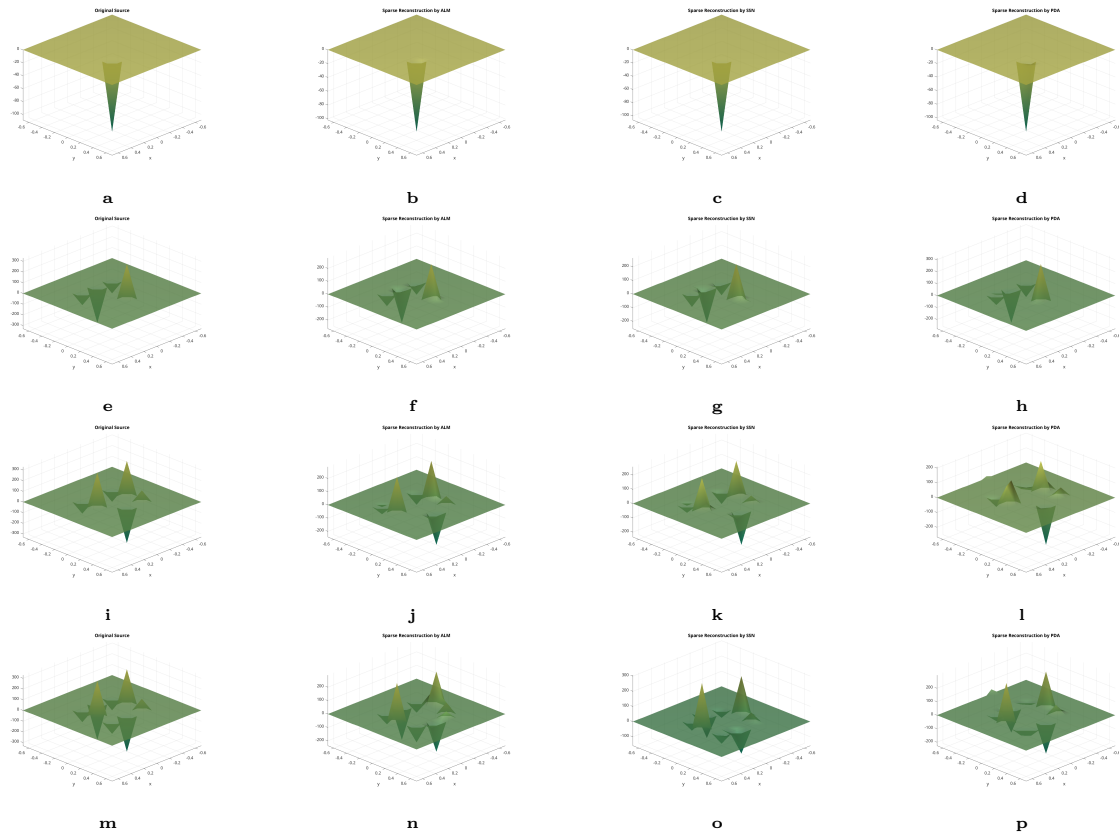


**Figure 3:** Reconstruction of sparse sources with multiple peaks in inhomogeneous media with  $k = 6$ . The information of the acoustic sources and the corresponding reconstruction algorithms are the same as in Figure 2.

**Table 1:** Comparisons of the running time and relative errors for ALM, SSN, and PDA algorithms with noise level 1%. This table corresponds to Figure 2 and Figure 3. The running times, i.e., “Times (s)” are only presented for the homogeneous cases as in Figure 2. The “N-error” and “N-error (in)” are relative errors for the corresponding homogeneous and inhomogeneous cases. The notations “one”, “four”, “six”, and “eight” corresponds to the sources with one, four, six, and eight peaks and are the same as in Figures 2 and 3. (ALM and SSN with  $\alpha = 9e-4$ ,  $\alpha_0 = 1e-7$ , and PDA with  $\alpha = 9e-5$ ,  $\alpha_0 = 1e-12$ ).

Methods	Sources	Time (s)	N-Error	N-Error (in)
ALM	one	8.77	6.30e-02	4.98e-02
	four	9.67	2.08e-01	7.69e-01
	six	11.19	1.01e-00	1.00e-00
	eight	9.13	1.09e-00	1.07e-00
SSN	one	8.62	1.93e-02	2.27e-02
	four	10.64	4.32e-01	1.37e-01
	six	8.09	9.57e-01	9.50e-01
	ten	10.11	1.10e-00	1.07e-00
PDA	one	17.12	6.99e-02	5.11e-2
	four	15.66	2.49e-01	1.47e-01
	six	16.71	9.09e-01	8.64e-01
	eight	16.31	1.19e-00	1.12e-00

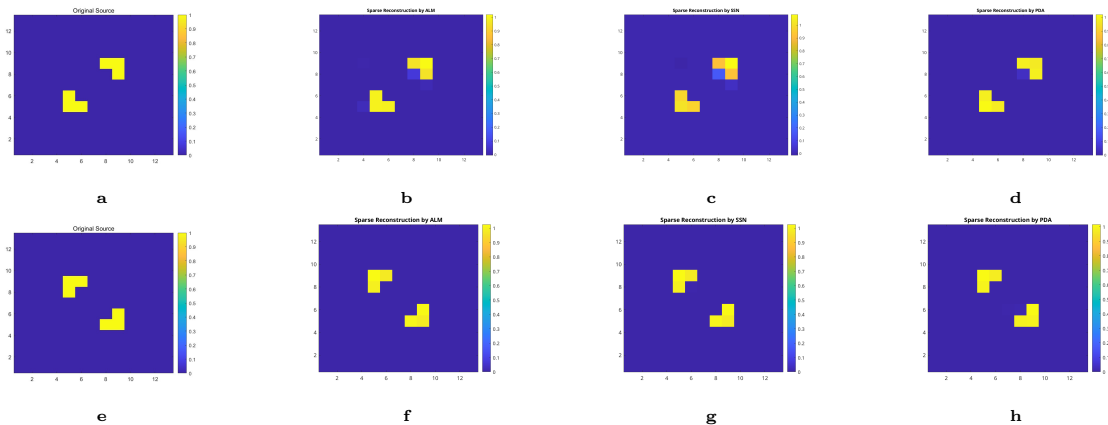


**Figure 4:** Reconstructions of strip-shaped sparse sources in homogeneous media with  $k = 4$ , noise level 0.1%, and  $\alpha = 2e-6$ ,  $\alpha_0 = 2e-8$ . The figures in the leftmost column are the original acoustic sources. The images in the second, the third from the left, and the rightmost columns are reconstructed results of ALM, SSN, and PDA, respectively. The images in the first and second rows are the sources with “skew diagonal” (the first row) and “diagonal” (the second row) types of strips, respectively.

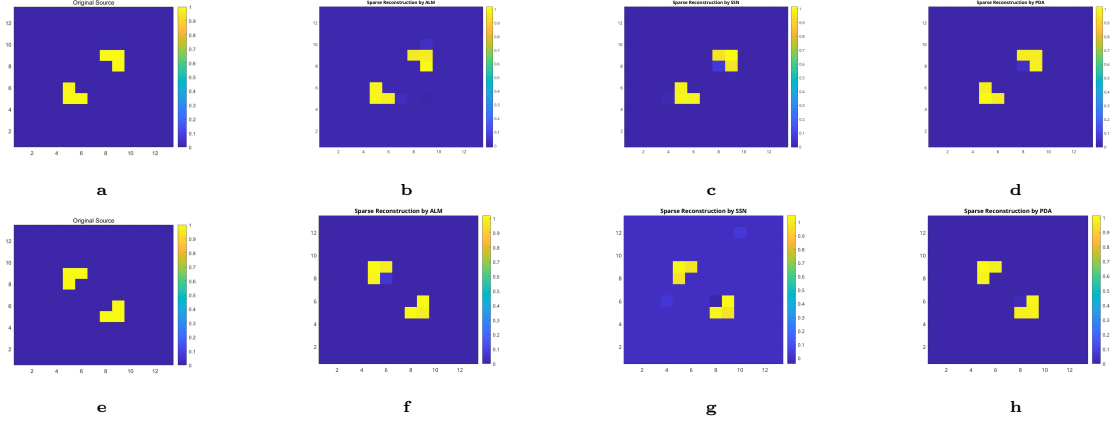


**Figure 5:** Reconstruction of strip-shaped sparse sources in inhomogeneous media with  $k = 4$ , noise level 0.1%, and  $\alpha = 2e-6$ ,  $\alpha_0 = 2e-8$ . The information of the acoustic sources and the corresponding reconstruction algorithms are the same as in Figure 4.

**Table 2:** Comparisons of the running time and relative errors for ALM, SSN, and PDA algorithms with noise level 0.1%, and  $\alpha = 2e-6$ , together with  $\alpha_0 = 2e-8$ . This table corresponds to Figure 2 and Figure 3. The running times, i.e., “Times (s)” are only presented for the homogeneous cases as in Figure 4. The “N-error” and “N-error (in)” are relative errors for the corresponding homogeneous and inhomogeneous cases. The notations “skew” and “diag” represent the “skew diagonal” and “diagonal” strips in Figures 4 and 5.

Methods	Sources	Time (s)	N-Error	N-Error (in)
ALM	skew	16.96	4.19e-02	2.30e-02
	diag	17.23	1.75e-02	4.18e-02
SSN	skew	11.07	9.18e-02	4.04e-02
	diag	11.72	1.79e-02	3.81e-02
PDA	skew	18.15	2.40e-02	2.49e-02
	diag	18.82	1.51e-02	1.70e-02

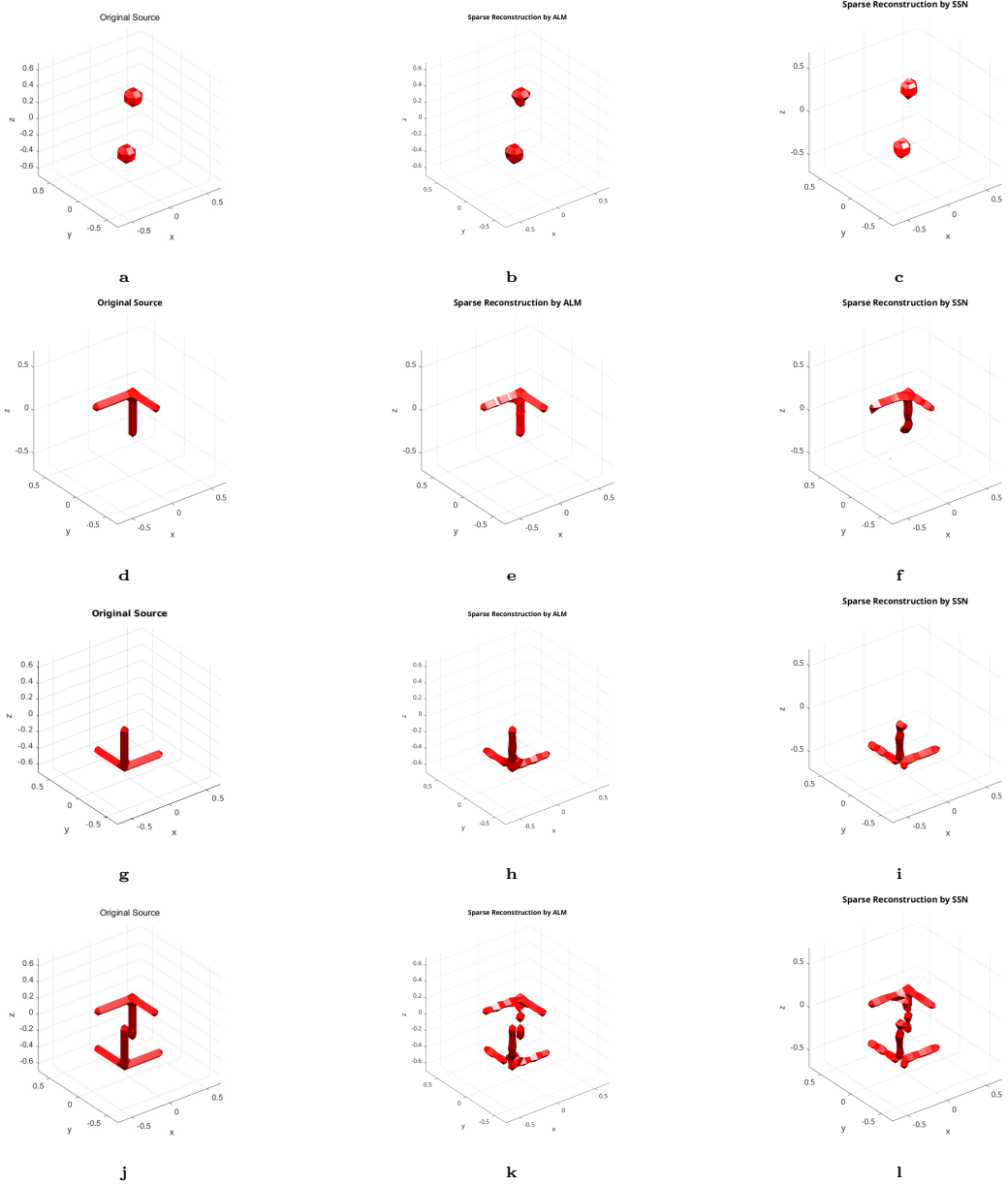


**Figure 6:** Reconstruction of 3-dimensional sparse sources in homogeneous media with  $k = 6$ , noise level 1%, and  $\alpha = 5e-7$  together with  $\alpha_0 = 2e-8$ . The solution is computed by  $-\lambda^{K_{\max}}$ . The figures in the leftmost column are the original acoustic sources. The images in the middle and the rightmost columns are reconstructed results of ALM and SSN, respectively. The images in the first, second, third, and fourth rows are the sources with the two balls, the right up tripod, the left down tripod, and the two tripods, respectively.

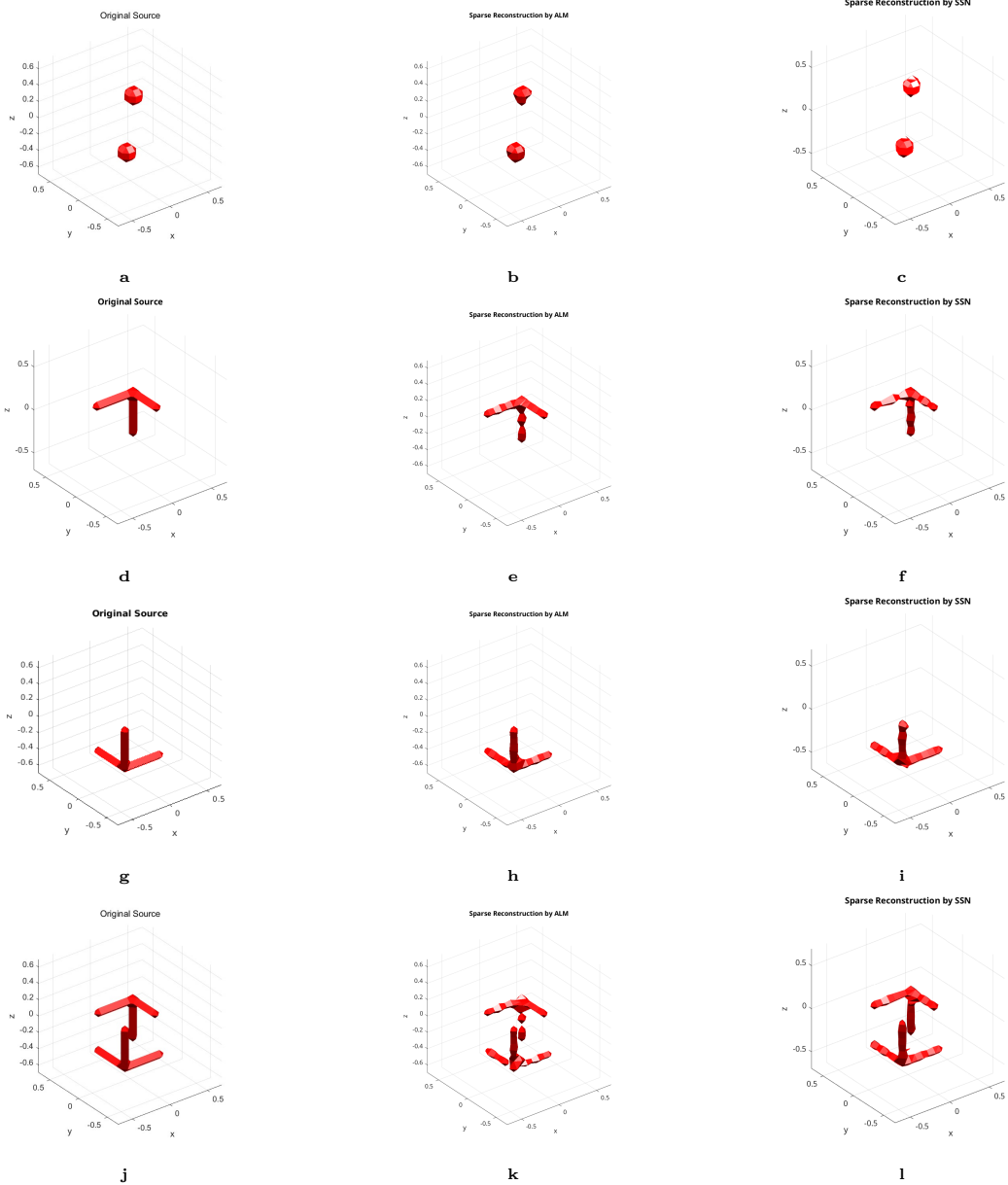


**Figure 7:** Reconstruction of 3-dimensional sparse sources in inhomogeneous media with  $k = 6$  and noise level 1%, and  $\alpha = 5\text{e-}7$  together with  $\alpha_0 = 2\text{e-}8$ . The solution is computed by  $-\lambda^{K_{\max}}$ . The information of the acoustic sources and the corresponding reconstruction algorithms are the same as in Figure 6.

**Table 3:** Experimental results for ALM and SSN methods under different scenarios and treatments, noise level 1%, and  $\alpha = 5e-7$  together with  $\alpha_0 = 2e-8$ . Here “N-Error” is the relative error for both homogeneous and inhomogeneous cases, corresponding to “homo” and “inhomo” in the table. The notations “two balls”, “two tripods”, “right up”, and “left down” represent the acoustic sources in the first to the fourth rows in Figure 6 or 7, respectively.

Methods	Sources	Medium	Time (s)	N-Error
ALM	two balls	homo	79.86	3.97e-01
	two balls	inhomo	87.71	3.99e-01
	two tripods	homo	82.29	4.26e-01
	two tripods	inhomo	88.84	4.96e-01
	right up	homo	79.49	3.14e-01
	right up	inhomo	87.01	2.78e-01
	left down	homo	78.36	3.03e-01
	left down	inhomo	88.69	2.55e-01
SSN	two balls	homo	1224.96	3.60e-01
	two balls	inhomo	1304.16	3.26e-01
	two tripods	homo	1195.87	4.47e-01
	two tripods	inhomo	1149.60	2.90e-01
	right up	homo	1139.21	4.35e-01
	right up	inhomo	1296.09	3.55e-01
	left down	homo	1228.42	4.01e-01
	left down	inhomo	1301.16	3.16e-01

**Table 4:** Relative reconstruction errors for ALM and SSN methods with noise level 0.01%, and  $\alpha = 1e-7$  together with  $\alpha_0 = 1e-9$ . The “N-error” and “N-error (in)” are relative errors for the corresponding homogeneous and inhomogeneous cases. The notations “two balls”, “right up”, and “left down” represent the acoustic sources in the first to the third rows in Figure 8 or 9, respectively. The running times are nearly the same to the 1% noise level cases as in Table and we omit here.

Methods	Sources	N-Error	N-Error (in)
ALM	two balls	1.27e-01	6.75e-02
	right up	1.40e-01	1.43e-02
	left down	7.33e-02	2.09e-02
SSN	two balls	3.72e-01	2.12e-01
	right up	1.35e-01	2.29e-01
	left down	4.07e-02	5.36e-03

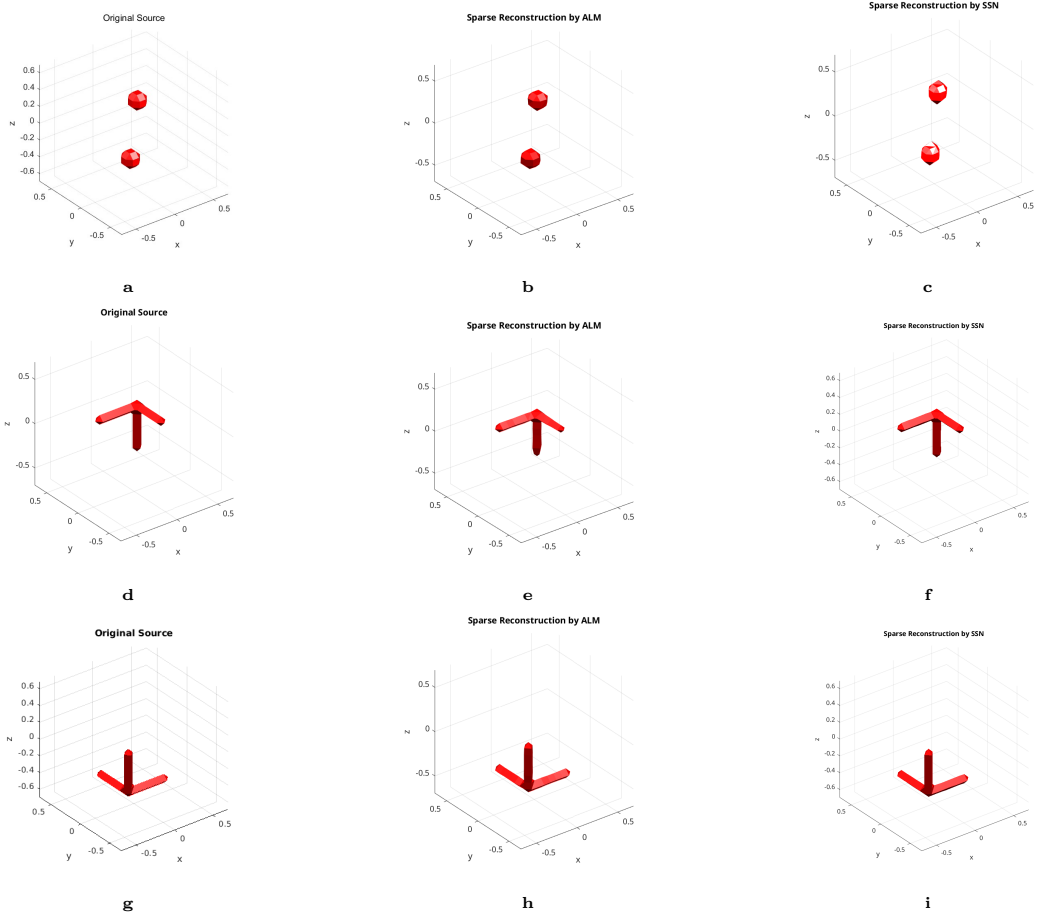


**Figure 8:** Reconstruction of 3-dimensional sparse sources in homogeneous media with  $k = 6$ , noise level 0.01%, and  $\alpha = 1e-7$  together with  $\alpha_0 = 1e-9$ . Reconstruction of 3-dimensional sparse sources in homogeneous media with  $k = 6$  and noise level 1%, and  $\alpha = 5e-7$  together with  $\alpha_0 = 2e-8$ . The figures in the leftmost column are the original acoustic sources. The images in the middle and the rightmost columns are reconstructed results of ALM and SSN, respectively. The images in the first, second, and third rows are the sources with the two balls, the right up tripod, and the left down tripod, respectively.

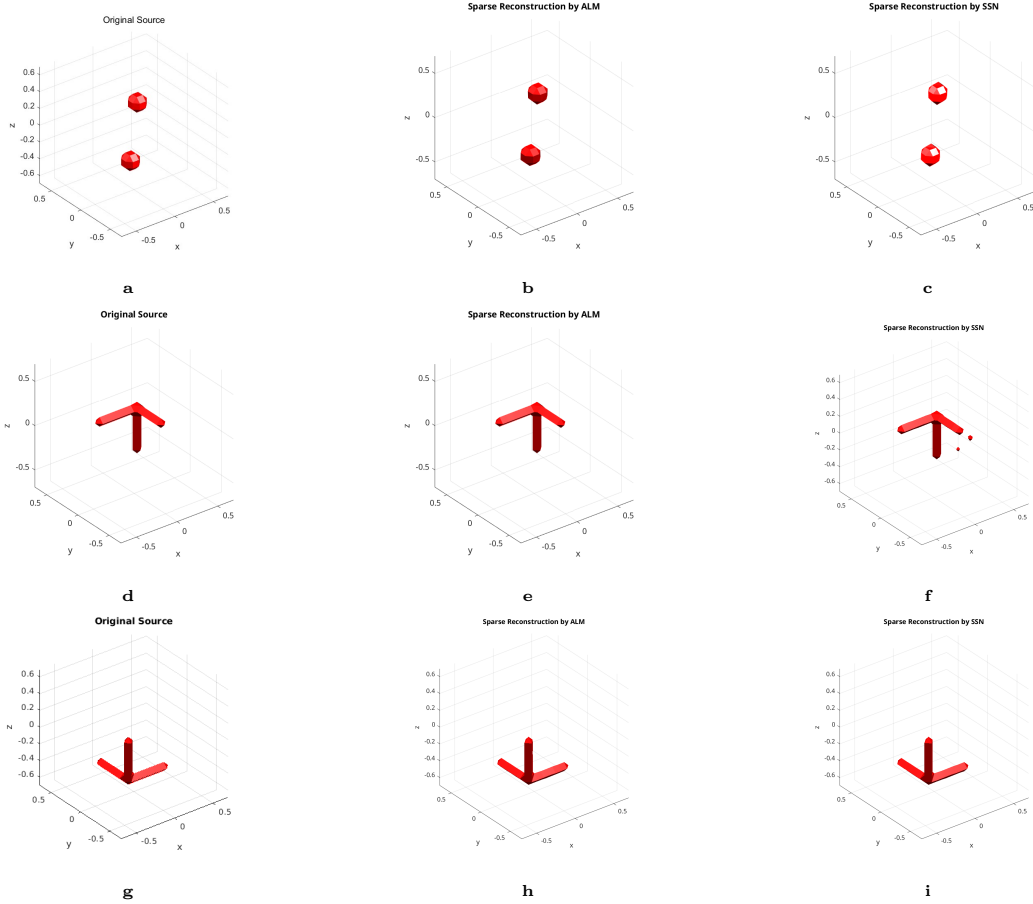


**Figure 9:** Reconstruction of 3-dimensional sparse sources in inhomogeneous media with  $k = 6$ , noise level 0.01%, and  $\alpha = 1e-7$  together with  $\alpha_0 = 1e-9$ . The information of the acoustic sources and the corresponding reconstruction algorithms are the same as in Figure 8.

## Acknowledgements

Nirui Tan and Hongpeng Sun acknowledge the support of the National Natural Science Foundation of China under grant No. 12271521, National Key R&D Program of China (2022ZD0116800), and Beijing Natural Science Foundation No. Z210001.

## References

- [1] G. S. Alberti, R. Petit, and M. Santacesaria, *Localization of Point Scatterers via Sparse Optimization on Measures*, SIAM J. Imaging Sciences, 17(3), 2024, pp. 1619–1649.
- [2] G. S. Alberti, M. Santacesaria, *Infinite-dimensional inverse problems with finite measurements*, Arch. Ration. Mech. Anal., 243 (2022), pp. 1–31.
- [3] A. Alzaalig, G. Hu, X. Liu, and J. Sun, *Fast acoustic source imaging using multi-frequency sparse data*, Inverse Problems 36 (2020) 025009 (18pp).
- [4] R. A. Adams, John J. F. Fournier, Sobolev Spaces, 2nd Edition, 2003, Elsevier Ltd.
- [5] G. Bao, J. Lin, F. Triki, *A multi-frequency inverse source problem*, J. Differential Equations, 249(2010), pp. 3443–3465.
- [6] G. Bao, P. Li, J. Lin, F. Triki, *Inverse scattering problems with multi-frequencies*, Inverse Problems, 31(2015), no. 9, 093001, 21 pp.
- [7] H. H. Bauschke, P. L. Combettes, Convex Analysis and Monotone Operator Theory in Hilbert Spaces, Springer Science+Business Media, LLC, second edition, 2017.
- [8] N. Bleistein, J. K. Cohen, *Nonuniqueness in the inverse source problem in acoustics and electromagnetics*, J. Math. Phys. 18, 1977, pp. 194–201.
- [9] K. Bredies, H. K. Pikkainen, *Inverse problems in spaces of measures*, ESAIM: COCV 19, pp. 190–218, 2013.
- [10] H. Brezis, Functional Analysis, Sobolev Spaces and Partial Differential Equations, Springer Science+Business Media, LLC 2011.
- [11] Weng C. Chew, Y. M. Wang, *Reconstruction of two-dimensional permittivity distribution using the distorted Born iterative method*, IEEE Transactions on Medical Imaging, 9(2), pp. 218–225, 1990.
- [12] Florian Bürgel, Kamil S. Kazmierski, and Armin Lechleiter, *A sparsity regularization and total variation based computational framework for the inverse medium problem in scattering*, Journal of Computational Physics, 339:1–30, 2017.

- [13] Florian Bürgel, Kamil S. Kazmierski, and Armin Lechleiter, *Algorithm 1001: IP-scatt—A MATLAB Toolbox for the Inverse Medium Problem in Scattering*, ACM Transactions on Mathematical Software (TOMS), Vol. 45(4), pp. 1-20.
- [14] A. Chambolle, T. Pock. *A first-order primal-dual algorithm for convex problems with applications to imaging*, J. Math. Imaging Vis., Vol. 40, No. 1, 2011.
- [15] E. Casas, C. Clason, K. Kunisch, *Approximation of elliptic control problems in measure spaces with sparse solutions*, SIAM J. Control Optim., 50(4), pp. 1735–1752, 2012.
- [16] C. Clason, K. Kunisch, *A duality-based approach to elliptic control problems in non-reflexive Banach spaces*, ESAIM: COCV, 17 pp. 243–266, 2011.
- [17] D. Colton, R. Kress, Inverse Acoustic and Electromagnetic Scattering Theory, Springer Science+Business Media New York, Third Edition, 2013.
- [18] D. Colton, P. Monk, *A linear sampling method for the detection of leukemia using microwaves*, SIAM J. Appl. Math., 58(3), pp. 926-941, 1998.
- [19] A. J. Devaney, E. A. Marengo, Mei Li, *Inverse source problem in nonhomogeneous background media*, SIAM J. Appl. Math., 67(5), (2007), pp. 1353–1378.
- [20] A. L. Dontchev, R. T. Rockafellar, Functions and Solution Mappings: A View from Variational Analysis, Second Edition, Springer Science+Business Media, New York 2014.
- [21] O. Dorn, H. Bertete-Aguirre, G.C. Papanicolaou, *A nonlinear inversion method for 3D electromagnetic imaging using adjoint fields*, Inverse Problems, 1999, 15, 1523.
- [22] O. Dorn, H. Bertete-Aguirre, G.C. Papanicolaou, *Adjoint Fields and Sensitivities for 3D Electromagnetic Imaging in Isotropic and Anisotropic Media*, 2008. In: Bonilla, L.L. (eds) Inverse Problems and Imaging. Lecture Notes in Mathematics, vol 1943. Springer, Berlin, Heidelberg.
- [23] M. Eller, N. P. Valdivia, *Acoustic source identification using multiple frequency information*, Inverse Problems, 25(2009), 115005 (20pp).
- [24] Andrew J. Hesford, Weng C. Chew, *A Frequency-Domain Formulation of the Fréchet Derivative to Exploit the Inherent Parallelism of the Distorted Born Iterative Method*, Waves in Random and Complex Media 16 (4): 495–508, 2006.
- [25] M. Hintermüller, K. Kunisch, *Total bounded variation regularization as a bilaterally constrained optimization problem*, SIAM J. Appl. Math, 64(4), pp. 1311–1333.
- [26] T. Hohage, *On the numerical solution of a three-dimensional inverse medium scattering problem*, Inverse Problems, 2001, 17, pp. 1743-1763.

- [27] T. Hohage, *Fast numerical solution of the electromagnetic medium scattering problem and applications to the inverse problem*, J. Comp. Phys. 214, pp. 224–238, 2006.
- [28] K. Ito, K. Kunisch, Lagrange Multiplier Approach to Variational Problems and Applications. SIAM, Philadelphia (2008)
- [29] M. Moghaddam, Weng C. Chew, M. Oristaglio, *Comparison of the born iterative method and tarantola's method for an electromagnetic time-domain inverse problem*, International Journal of Imaging Systems and Technology, 3(4), 318-333, 1991.
- [30] J. Sylvester, *Notions of support for far fields*, Inverse Problems, 22, (2006), pp. 1273–1288.
- [31] Gennadi Vainikko, *Fast Solvers of the Lippmann-Schwinger Equation*, In Robert P. Gilbert, Joji Kajiwara, and Yongzhi S. Xu, editors, Direct and Inverse Problems of Mathematical Physics, pages 423–440. Springer, Boston, 2000.
- [32] X. Xiang, H. Sun, Sparse reconstructions of acoustic source for inverse scattering problems in measure space, 2020, Inverse Problems, 36 035004.
- [33] M. Fortin, R. Glowinski (eds.), Augmented Lagrangian Methods: Applications to the Solution of Boundary Value Problems, North-Holland, Amsterdam, 1983.
- [34] R. Glowinski, S. Osher, W. Yin (eds.), Splitting Methods in Communication, Imaging, Science, and Engineering, Springer, 2016.
- [35] M. R. Hestenes, *Multiplier and gradient methods*, J. Optim. Theory Appl., 4, pp. 303–320, 1968
- [36] K. Ito, K. Kunisch, *An active set strategy based on the augmented Lagrangian formulation for image restoration*, RAIRO, Math. Mod. and Num. Analysis, 33(1), pp. 1–21, 1999.
- [37] X. Li, D. Sun, C. Toh, *A highly efficient semismooth Newton augmented Lagrangian method for solving lasso problems*, SIAM J. Optim., 28(1), pp. 433–458, 2018.
- [38] M. J. D. Powell, *A method for nonlinear constraints in minimization problems*, in Optimization, R. Fletcher, ed., Academic Press, New York, pp. 283–298, 1968.
- [39] R. F. Remis, P. M. van den Berg, *On the equivalence of the Newton-Kantorovich and distorted Born methods*, Inverse Problems, 16 L1-L4, 2000.
- [40] S. M. Robinson, *Some continuity properties of polyhedral multifunctions*, in Mathematical Programming at Oberwolfach, Math. Program. Stud., Springer, Berlin, Heidelberg, pp. 206–214, 1981.

- [41] R. T. Rockafellar, *Monotone operators and the proximal point algorithm*, SIAM J. Control Optim., 14(5), pp. 877–898, 1976.
- [42] R. T. Rockafellar, *Augmented Lagrangians and applications of the proximal point algorithm in convex programming*, Math. Oper. Res., 1(2), pp. 97-116, 1976.
- [43] S. Scholtes, Introduction to Piecewise Differentiable Equations, Springer Briefs in Optimization, Springer, New York, 2012.
- [44] G. Stadler, *Semismooth Newton and augmented Lagrangian methods for a simplified friction problem*, SIAM J. Optim., 15(1), pp. 39–62, 2004.
- [45] H. Sun, *An Investigation on Semismooth Newton based Augmented Lagrangian Method for Image Restoration*, J. Sci. Comput. 92(82), 2022.
- [46] H. Sun, *An efficient augmented Lagrangian method with semismooth Newton solver for total generalized variation*, Inverse Problems and Imaging, 2023, 17(2): 381-405.
- [47] A. Tarantola, Inverse Problem Theory and Methods for Model Parameter Estimation, SIAM, 2005.
- [48] R. Tomioka and M. Sugiyama, *Dual-augmented Lagrangian method for efficient sparse reconstruction*, in IEEE Signal Processing Letters, 16(12), pp. 1067–1070, Dec. 2009.
- [49] M. Ulbrich, Semismooth Newton Methods for Variational Inequalities and Constrained Optimization Problems in Function Spaces, MOS-SIAM Series on Optimization, 2011.
- [50] X. Zhao, D. Sun, K. Toh, *A Newton-CG augmented Lagrangian method for semidefinite programming*, SIAM J. Optim., 20(4), pp. 1737–1765, 2010.